NASA Contractor Report 194933

ICASE Report No. 94-47

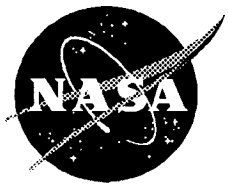

ICASE

NONLINEAR STABILITY OF OSCILLATORY CORE-ANNULAR FLOW: A GENERALIZED KURAMOTO-SIVASHINSKY EQUATION WITH TIME PERIODIC COEFFICIENTS

Adrian V. Coward
Demetrios T. Papageorgiou
Yiorgos S. Smyrlis

Contract NAS1-19480
July 1994

Institute for Computer Applications in Science and Engineering
NASA Langley Research Center
Hampton, VA 23681-0001

Operated by Universities Space Research Association

ICASE Fluid Mechanics

Due to increasing research being conducted at ICASE in the field of fluid mechanics, future ICASE reports in this area of research will be printed with a green cover. Applied and numerical mathematics reports will have the familiar blue cover, while computer science reports will have yellow covers. In all other aspects the reports will remain the same; in particular, they will continue to be submitted to the appropriate journals or conferences for formal publication.

Nonlinear stability of oscillatory core-annular flow: A generalized Kuramoto-Sivashinsky equation with time periodic coefficients.

Adrian V. Coward * Demetrios T. Papageorgiou † Yiorgos S. Smyrlis ‡

Abstract

In this paper the nonlinear stability of two-phase core-annular flow in a pipe is examined when the acting pressure gradient is modulated by time harmonic oscillations and viscosity stratification and interfacial tension is present. An exact solution of the Navier-Stokes equations is used as the background state to develop an asymptotic theory valid for thin annular layers, which leads to a novel nonlinear evolution describing the spatio-temporal evolution of the interface. The evolution equation is an extension of the equation found for constant pressure gradients and generalizes the Kuramoto-Sivashinsky equation with dispersive effects found by Papageorgiou, Maldarelli & Rumschitzki, Phys. Fluids A 2(3), 1990, pp.340-352, to a similar system with time periodic coefficients. The distinct regimes of slow and moderate flow are considered and the corresponding evolution is derived. Certain solutions are described analytically in the neighborhood of the first bifurcation point by use of multiple scales asymptotics. Extensive numerical experiments, using dynamical systems ideas, are carried out in order to evaluate the effect of the oscillatory pressure gradient on the solutions in the presence of a constant pressure gradient.

*Department of Mathematics, Manchester University, Manchester, U.K. Research supported by NATO grant CRG 920097.

†Department of Mathematics, Center for Applied Mathematics and Statistics, New Jersey Institute of Technology, Newark NJ 07102. Research was supported by the National Aeronautics and Space Administration under NASA Contract No. NAS1-19480 while the author was in residence at the Institute for Computer Applications in Science and Engineering (ICASE), M/S 132C, NASA Langley Research Center, Hampton, VA 23681; also by by grants NATO CRG 920097, and SBR NJIT-93.

‡Department of Mathematics, University of Manchester, Manchester, U.K. & Department of Mathematics and Statistics, University of Cyprus, Nicosia, Cyprus. Research supported by NATO grant CRG 920097.

1 Introduction

Core annular flows (CAFs) are immiscible two-fluid flows in a cylindrical tube in which one fluid moves through the tube core and the other liquid occupies the annular region surrounding the core. If a constant pressure gradient causes the flow, an exact solution of the Navier-Stokes equations is available with the interface between the two fluids being perfectly cylindrical. A considerable amount of research has been applied in an effort to characterize the instability of such perfect CAF arrangements. There are many technological applications where the CAF serves as a useful model for the dynamics, such as, lubricated pipelining, concurrent flows in packed beds, coating processes, and liquid-liquid displacements in the presence of a wall-wetting layer in porous media, to mention a few. The important theoretical question lies in the prediction of whether the core-annular geometry will be realized or whether the flow will break up into a slug or emulsion flow.

Experimental and theoretical studies indicate that the main physical parameters that affect the stability are capillary forces, viscosity differences and density differences between the phases. The effect of viscosity differences was first studied by Yih (1967) for the stability of two-phase plane Couette-Poiseuille flow; he derived analytical expressions for the growth-rates of linear perturbations in the long-wave limit (i.e. disturbances with wavelengths which are much larger than the plate separation distance) from which the following conclusions are inferred: If the two fluids have different viscosities an instability is possible at any value of the Reynolds number, however small (the instability is not associated with high Reynolds numbers alone). The flow is stable (for long waves at least) if the less viscous fluid occupies the thinner of the two layers and unstable for converse arrangements. Hooper (1985) and Hooper & Boyd (1983) generalized Yih's results for semi-infinite and infinite two-phase Couette flows which are useful models in studying short-wave instabilities. Renardy (1985) addressed the problem numerically and shows that in planar Couette flow short and intermediate waves can become unstable in parameter regimes where the long wave analysis predicts stability.

In cylindrical geometries the situation is different in that surface tension acts to destabilize interfacial waves longer than the core diameter even in the absence of flow (Tomotika (1935), Goren (1962)). For flow in a core-annular arrangement, Hickox (1971) analyzed long wavelength perturbations and found instability whenever the annular fluid is more viscous than the core fluid. More complete linear stability analyses have been carried out in a series of articles by Joseph, Renardy & Renardy (1984), Preziosi, Chen & Joseph (1989), Hu & Joseph (1989), Hu, Lundgren & Joseph (1990), Chen, Bai & Joseph (1990), Bai, Chen & Joseph (1992), Chen & Joseph (1991) & Chen (1992). These authors use numerical and long-wave techniques to produce a detailed picture of the linear stability to mainly axially symmetric perturbations. The authors find that there are essentially two competing mechanisms at play: (i) Capillary forces which destabilize long waves and are, to leading order in the interfacial deflection, independent of the basic flow, (ii) Viscosity differences which provide a jump in the leading order axial velocity perturbation which destabilizes short waves and can also destabilize long waves when the annular fluid is the more viscous (long waves are stabilized by these forces if the core fluid is more viscous). The studies detailed above show that the interaction of these mechanisms can produce a window of linear stability which can be explained as follows: in situations when the annular fluid thickness is much smaller than the core radius and its viscosity smaller than that of the core fluid, the viscosity difference mechanism provided by the axial velocity jump (see above) causes a stabilization of long waves (which would have been unstable otherwise due to the capillary instability) at sufficiently large Reynolds numbers. As the Reynolds number increases further the flow becomes unstable to the short wave mechanism. It is established, therefore, that the flow parameters can be chosen so that the flow is linearly

stable to perturbations of all wavelengths. For a complete and up to date account of theoretical and experimental results and their comparisons see the texts by Joseph & Renardy (1993).

The nonlinear stability of CAFs when capillary forces are important, has been considered by Papageorgiou, Maldarelli & Rumschitzki (1990) (hereafter refered to as PMR). This was done in the limit of a thin annular layer by a systematic asymptotic expansion procedure on the Navier-Stokes equations. In this limit the film dynamics reduce to those given by lubrication theory and a matching can be achieved analytically between film and core dynamics to produce an evolution equation for the scaled interfacial amplitude $\eta(t,z)$ where t is time and z axial distance, which can be written as

$$\eta_t + \eta\eta_z + \eta_{zz} + \nu\eta_{zzzz} + (1 - \frac{1}{m})\mathcal{L}(u) = 0, \tag{1}$$

where $0 < \nu < 1$ is a parameter inversely proportional to the square of the wavelength and m is the viscosity ratio of core and film fluids. The last term arises due to viscosity differences and is a linear pseudo-differential operator with a known spectrum (see PMR and also below). The validity of the lubrication approximation is given by Georgiou, Maldarelli, Papageorgiou & Rumschitzki (1992) who analyze the linear stability dispersion relation in the limit of a thin annular fluid and identify the linear terms of (1) exactly to leading order. Further more, it is shown that the lubrication approximation agrees with the numerically computed eigenvalues for annulus to core radius ratios (denoted by ϵ) as large as 0.2, a finding which implies that (1) may be a useful approximation for finite but small ϵ (note that ϵ can easily be re-introduced in (1)).

When $m = 1$, (1) reduces to the Kuramoto-Sivashinsky equation which has been widely studied both analytically (see for example Nicolaenko, Scheurer & Temam (1985), Constantin, Foias, Nicolaenko & Temam (1988)) and computationally (Sivashinsky & Michelson (1980), Hyman & Nicolaenko (1986), Hyman, Nicolaenko & Zaleski (1986), Kevrekidis, Nicolaenko & Scovel (1990), Papageorgiou & Smyrlis (1990) (referred to as PS), Smyrlis & Papageorgiou (1991) (referred to as SP) among others.) These studies show that the dynamics exhibits a low-modal behavior and complexity sets in as ν decreases below unity. PS and SP showed numerically the existence of a period-doubling route to chaos according to the Feigenbaum scenario (see Feigenbaum (1980)) and have computed a Feigenbaum number from their numerical results with a three digit accuracy. It is noted that such results are reproducible with a fairly low-dimensional representation of the PDE; the number of modes required to capture the dynamics was found (empirically by extensive numerical experiments) to be a few more than $\nu^{-\frac{1}{2}}$, the number of linearly unstable 2π-periodic waves.

An extension of the analysis of PMR to include asymmetric interfacial deflections and in particular the effects of pipe rotation, has been carried out by Coward & Hall (1993). A spatially two-dimensional version of (1) is derived, analyzed and solved numerically. In the absence of rotation it is found that asymmetric initial conditions lead, after a long time, to axially symmetric motions. When rotation is present, however, the most unstable linear wave has azimuthal dependence and as a consequence the nonlinear solutions are two-dimensional.

If the annular and core fluids have different viscosities ($m \neq 1$) the following behavior has been established in PMR for (1) and by Coward and Hall for the higher dimensional equation: Viscosity differences cause dispersive effects. If $|1 - 1/m|$ exceeds a certain value (which depends on ν), the long-time evolution produces nonlinear traveling waves whose amplitude grows with the amount of dispersion. In particular this is established for situations where in the absence of dispersive effects ($m = 1$) the KS equation produces spatio-temporal chaos. The conclusion is that dispersion (viscosity differences) can organize chaotic motions into well-defined stable travelling wave solutions.

The present work extends the research cited above to CAFs which have driving axial pressure gradients with time periodic modulations. Such flows are easily achieved in practice by using a pump to drive the flow. Time periodic two-phase flows have received very little attention. The stability of a single layer of fluid on a flat plate which is performing time periodic oscillations horizontally has been studied by Yih (1968) using a long wave analysis coupled with a Floquet theory. Von Kerczek (1987) studied the corresponding problem when the plate is vertical and performs oscillations along its plane, by solving the Floquet eigenvalue problem numerically for different wavenumbers. Both investigations indicate that the flow can be stabilized by the periodic oscillations. Coward & Papageorgiou (1994) study the stability of two-phase Couette flow when the upper plate has a horizontal velocity which comprises of a constant component and a time periodic modulation. The problem is more involved due to the presence of two fluids, and analytical expressions have been found for the Floquet exponents (growth rates) in the limit of long waves. The main finding is that the oscillations can completely stabilize otherwise unstable flows, but at the same time can make unstable flows, in certain parameter regimes, even more unstable.

This article considers the nonlinear stability of an oscillatory CAF. An exact laminar parallel flow solution of the Navier-Stokes equations can be found for an annulus of arbitrary thickness which bounds the core with a perfectly cylindrical interface. This time-periodic flow is used as the undisturbed state in the development of an asymptotic theory using ϵ as the small parameter in order to develop a nonlinear evolution equation for the interfacial deflections which takes into account the effects of both capillary forces and the background harmonic fluctuations. The scaled evolution equation, using the notation of (1), which is valid for low frequency modulations, takes the form

$$\eta_t + (1 + \Delta\cos(\Omega t))\eta\eta_z + \eta_{zz} + \nu\eta_{zzzz} + (1 - \frac{1}{m})\mathcal{L}(u) = 0, \tag{2}$$

where Δ is the nondimensional amplitude of the background pressure gradient modulations and Ω their scaled frequency. This equation is studied analytically and computationally in order to characterize the effect of the background modulations on the dynamics.

The paper is organized as follows. In Section 2 we formulate the problem, write down the unperturbed time periodic flow and give the exact nonlinear equations of motion along with the interfacial conditions. In Section 3 an asymptotic analysis of these equations is carried out in the limit $\epsilon \to 0$ and two canonical regimes are analyzed to produce equations of the form (2) with different pseudo-differential operators which correspond to slow flow with moderate surface tension and moderate flow with large surface tension, respectively. In Section 4 the equations are analyzed near the point $\nu = 1$ which corresponds to the minimum wavelength which first becomes unstable (the first bifurcation). A multiple scales analysis is employed to describe the solution and the analytical results are compared to numerical solutions with good agreement. Section 5 is devoted to extensive numerical experiments of (2) for values of $\nu < 1$ where more than just two or three modes are relevent. We address questions such as the effect of the background oscillations on (i) steady states of KS, (ii) time periodic states, (iii) chaotic states, (iv) travelling wave solutions, and (v) travelling nonlinear dispersive states. Section 6 contains the conclusions of this study and discusses future work.

2 Formulation of the problem

A fixed circular cylinder of constant radius $r^* = R_2$ contains two incompressible, immiscible fluids which occupy concentric core and annular regions. These fluids have a common density ρ, but different viscosities μ_1 and μ_2, where the subscript corresponds to regions $0 \leq r^* \leq R_1$ and $R_1 \leq r^* \leq R_2$ respectively.

Polar coordinates are used so that $r^* = 0$ is aligned parallel to the $\mathbf{z}$ axis and an unsteady axial pressure gradient

$$\nabla \overline{P}^* = -\left(F + \Lambda \cos\left(\omega t^*\right)\right) \hat{\mathbf{z}},$$

is applied to both fluids. In the analysis that follows gravity is neglected if the pipe is horizontal and can be included quite easily in vertical arrangements (see [[8]], and [[1]]).

The undisturbed state is a parallel time dependent flow of the form $\overline{\mathbf{U}}^*_{1,2}\left(r^*, t^*\right) = \left(0, 0, \overline{W}^*_{1,2}(t, r)\right)$ and is governed by following form of the Navier-Stokes equations in the core and annular layers respectively

$$\begin{aligned}
\rho \frac{\partial \overline{W}^*_1}{\partial t^*} &= F + \Lambda \cos\left(\omega t^*\right) + \mu_1 \left(\frac{\partial^2 \overline{W}^*_1}{\partial r^{*2}} + \frac{1}{r^*} \frac{\partial \overline{W}^*_1}{\partial r^*} \right), \\
\rho \frac{\partial \overline{W}^*_2}{\partial t^*} &= F + \Lambda \cos\left(\omega t^*\right) + \mu_2 \left(\frac{\partial^2 \overline{W}^*_2}{\partial r^{*2}} + \frac{1}{r^*} \frac{\partial \overline{W}^*_2}{\partial r^*} \right).
\end{aligned}$$

The annular fluid satisfies a no-slip velocity condition at the cylinder wall and the core velocity must remain finite at the axis of the cylinder. The interface conditions dictate that velocity and tangential stress be continuous, so that

$$\begin{aligned}
\overline{W}^*_1\left(r^* = R_1\right) &= \overline{W}^*_2\left(r^* = R_1\right), \\
\mu_1 \frac{\partial \overline{W}^*_1}{\partial r^*}\left(r^* = R_1\right) &= \mu_2 \frac{\partial \overline{W}^*_2}{\partial r^*}\left(r^* = R_1\right).
\end{aligned}$$

The surface tension σ between the fluids induces a jump in the normal stress at the interface,

$$\overline{P}^*_1 = \overline{P}^*_2 + \frac{\sigma}{R_1}, \qquad \text{at } r^* = R_1.$$

These equations and boundary conditions admit the following solutions

$$\overline{W}^*_1 = \frac{F\left(R_1^2 - r^{*2}\right)}{4\mu_1} + \frac{F\left(R_2^2 - R_1^2\right)}{4\mu_2} + \Re\left\{ \frac{i\Lambda}{\rho\omega} \left[A I_0\left(\beta_1 r^*\right) - 1 \right] \exp\left(i\omega t^*\right) \right\}, \tag{3}$$

$$\overline{W}^*_2 = \frac{F\left(R_2^2 - r^{*2}\right)}{4\mu_2} + \Re\left\{ \frac{i\Lambda}{\rho\omega} \left[B I_0\left(\beta_2 r^*\right) + C K_0\left(\beta_2 r^*\right) - 1 \right] \exp\left(i\omega t^*\right) \right\}. \tag{4}$$

where $\beta_1 = (1+i)\left(\omega\rho/2\mu_1\right)^{\frac{1}{2}}$ and $\beta_2 = (1+i)\left(\omega\rho/2\mu_2\right)^{\frac{1}{2}}$, I_n and K_n are nth order modified Bessel functions and $\Re$ denotes the real part of a complex number. The three constants A, B, C in (3) and (4) are given by the solution of

$$\begin{aligned}
A I_0\left(\beta_1 R_1\right) &= B I_0\left(\beta_2 R_1\right) + C K_0\left(\beta_2 R_1\right), \\
\mu_1^{\frac{1}{2}} A I_1\left(\beta_1 R_1\right) &= \mu_2^{\frac{1}{2}} \left[B I_1\left(\beta_2 R_1\right) - C K_1\left(\beta_2 R_1\right) \right], \\
1 &= B I_0\left(\beta_2 R_2\right) + C K_0\left(\beta_2 R_2\right),
\end{aligned}$$

and

$$\begin{aligned}
A &= \mu_2^{\frac{1}{2}} \left[I_1\left(\beta_2 R_1\right) K_0\left(\beta_2 R_1\right) + K_1\left(\beta_2 R_1\right) I_0\left(\beta_2 R_1\right) \right] \\
&\times \left\{ \left[\mu_2^{\frac{1}{2}} I_1\left(\beta_2 R_1\right) I_0\left(\beta_1 R_1\right) - \mu_1^{\frac{1}{2}} I_0\left(\beta_2 R_1\right) I_1\left(\beta_1 R_1\right) \right] K_0\left(\beta_2 R_2\right) \right.
\end{aligned}$$

$$+ \quad \left[\mu_2^{\frac{1}{2}} I_0(\beta_1 R_1) K_1(\beta_2 R_1) + \mu_1^{\frac{1}{2}} K_0(\beta_2 R_1) I_1(\beta_1 R_1)\right] I_0(\beta_2 R_2)\Big\}^{-1}, \tag{5}$$

$$B = \left[\mu_2^{\frac{1}{2}} I_0(\beta_1 R_1) K_1(\beta_2 R_1) + \mu_1^{\frac{1}{2}} K_0(\beta_2 R_1) I_1(\beta_1 R_1)\right]$$
$$\times \left\{\left[\mu_2^{\frac{1}{2}} I_1(\beta_2 R_1) I_0(\beta_1 R_1) - \mu_1^{\frac{1}{2}} I_0(\beta_2 R_1) I_1(\beta_1 R_1)\right] K_0(\beta_2 R_2)\right.$$
$$\left. + \left[\mu_2^{\frac{1}{2}} I_0(\beta_1 R_1) K_1(\beta_2 R_1) + \mu_1^{\frac{1}{2}} K_0(\beta_2 R_1) I_1(\beta_1 R_1)\right] I_0(\beta_2 R_2)\right\}^{-1}, \tag{6}$$

$$C = \left[\mu_2^{\frac{1}{2}} I_1(\beta_2 R_1) I_0(\beta_1 R_1) - \mu_1^{\frac{1}{2}} I_0(\beta_2 R_1) I_1(\beta_1 R_1)\right]$$
$$\times \left\{\left[\mu_2^{\frac{1}{2}} I_1(\beta_2 R_1) I_0(\beta_1 R_1) - \mu_1^{\frac{1}{2}} I_0(\beta_2 R_1) I_1(\beta_1 R_1)\right] K_0(\beta_2 R_2)\right.$$
$$\left. + \left[\mu_2^{\frac{1}{2}} I_0(\beta_1 R_1) K_1(\beta_2 R_1) + \mu_1^{\frac{1}{2}} K_0(\beta_2 R_1) I_1(\beta_1 R_1)\right] I_0(\beta_2 R_2)\right\}^{-1}. \tag{7}$$

We now non-dimensionalize fluid velocities by W_0, the basic steady flow evaluated at the axis of the core (see (3))

$$W_0 = \frac{F}{4\mu_1\mu_2}\left[R_1^2(\mu_2 - \mu_1) + R_2^2\mu_1\right].$$

The length, time and pressure scalings are R_1, $R_1 W_0^{-1}$, and ρW_0^2 respectively, and we define the following non-dimensional parameters:

$$a = \frac{R_2}{R_1}, \qquad m = \frac{\mu_2}{\mu_1}, \qquad \Omega = \frac{\omega R_1}{W_0},$$
$$R_e = \frac{W_0 R_1 \rho}{\mu_1}, \qquad \Delta = \frac{\Lambda R_1 R_e}{\rho W_0^2}, \qquad \beta = (1+i)\left(\frac{R_e\Omega}{2}\right)^{\frac{1}{2}},$$

The non-dimensional groups above represent the thickness of the undisturbed annular fluid, the viscosity ratio between film and core fluids, the non-dimensional frequency of the backgound oscillatory pressure gradient, a Reynolds number based on core variables, a non-dimensional amplitude of the backgound forcing and the Stokes layer thickness (proportional to $|\beta|^{-\frac{1}{2}}$. The non-dimensional form of the exact solution is

$$\overline{W}_1(r,t) = 1 - \frac{mr^2}{a^2+m-1} + \Re\left\{\frac{i\Delta}{\Omega R_e}\left[AI_0(\beta r) - 1\right]e^{(i\Omega t)}\right\}, \tag{8}$$

$$\overline{W}_2(r,t) = \frac{a^2-r^2}{a^2+m-1} + \Re\left\{\frac{i\Delta}{\Omega R_e}\left[BI_0\left(\frac{\beta r}{m^{\frac{1}{2}}}\right) + CK_0\left(\frac{\beta r}{m^{\frac{1}{2}}}\right) - 1\right]e^{(i\Omega t)}\right\}. \tag{9}$$

In the expressions (8) and (9) the constants A, B, C are the non-dimensional versions of (5), (6) and (7) and are obtained by the replacements $\mu_1 \to 1$, $\mu_2 \to m$, $\beta_1 R_1 \to \beta$ and $\beta_2 R_1 \to \beta\sqrt{m}a$ and $\beta_2 R_1 \to \sqrt{m}\beta$. Note also that when $\Delta = 0$ the steady problem is recovered as expected.

Consider next a general unsteady axisymmetric CAF so that the velocity in regions $j = 1, 2$ is given by $(U, V, W)_j(r, z, t)$ with the interface positioned at $r = S(z, t)$. The Navier-Stokes equations in the core are

$$\frac{\partial U_1}{\partial t} + U_1\frac{\partial U_1}{\partial r} + W_1\frac{\partial U_1}{\partial z} + \frac{\partial P_1}{\partial r} = \frac{1}{R_e}\left(\frac{\partial^2 U_1}{\partial r^2} + \frac{1}{r}\frac{\partial U_1}{\partial r} + \frac{\partial^2 U_1}{\partial z^2} - \frac{U_1}{r^2}\right), \tag{10}$$

$$\frac{\partial W_1}{\partial t} + U_1\frac{\partial W_1}{\partial r} + W_1\frac{\partial W_1}{\partial z} + \frac{\partial P_1}{\partial r} = \frac{1}{R_e}\left(\frac{\partial^2 W_1}{\partial r^2} + \frac{1}{r}\frac{\partial W_1}{\partial r} + \frac{\partial^2 W_1}{\partial z^2}\right), \tag{11}$$

and in the annular region

$$\frac{\partial U_2}{\partial t}+U_2\frac{\partial U_2}{\partial r}+W_2\frac{\partial U_2}{\partial z}+\frac{\partial P_2}{\partial r} = \frac{m}{R_e}\left(\frac{\partial^2 U_2}{\partial r^2}+\frac{1}{r}\frac{\partial U_2}{\partial r}+\frac{\partial^2 U_2}{\partial z^2}-\frac{U_2}{r^2}\right), \tag{12}$$

$$\frac{\partial W_2}{\partial t}+U_2\frac{\partial W_2}{\partial r}+W_2\frac{\partial W_2}{\partial z}+\frac{\partial P_2}{\partial r} = \frac{m}{R_e}\left(\frac{\partial^2 W_2}{\partial r^2}+\frac{1}{r}\frac{\partial W_2}{\partial r}+\frac{\partial^2 W_2}{\partial z^2}\right). \tag{13}$$

The equation of continuity in the core and annulus reads

$$\frac{1}{r}\frac{\partial (rU_j)}{\partial r}+\frac{\partial W_j}{\partial z}=0, \qquad j=1,2. \tag{14}$$

The velocity (U_2, V_2, W_2) satisfies no-slip at the cylinder wall and (U_1, V_1, W_1) must remain finite at the axis of the core. Using the notation

$$[(\cdot)]_2^1 = (\cdot)_1-(\cdot)_2\,,$$

$$R_{ej} = \begin{cases} R_e & j=1 \\ R_e m^{-1} & j=2 \end{cases},$$

the continuity of radial velocities, axial velocities, tangential and normal stresses at the interface are

$$[U_j]_2^1 = 0,$$

$$[W_j]_2^1 = 0,$$

$$\left[\frac{1}{R_{ej}}\left(\frac{\partial U_j}{\partial z}+\frac{\partial W_j}{\partial r}\right)\left(1-\left(\frac{\partial S}{\partial z}\right)^2\right)+\frac{2}{R_{ej}}\left(\frac{\partial U_j}{\partial r}-\frac{\partial W_j}{\partial z}\right)\frac{\partial S}{\partial z}\right]_2^1 = 0,$$

$$\left[P_j-\frac{2}{R_{ej}}\frac{\partial U_j}{\partial r}+\left(P_j-\frac{2}{R_{ej}}\frac{\partial W_j}{\partial z}\right)\left(\frac{\partial S}{\partial z}\right)^2+\frac{2}{R_{ej}}\left(\frac{\partial U_j}{\partial z}+\frac{\partial W_j}{\partial r}\right)\frac{\partial S}{\partial z}\right]_2^1 +$$

$$\frac{J}{R_e^2}\left(\frac{\partial^2 S}{\partial z^2}-\frac{1}{S}\left(1+\left(\frac{\partial S}{\partial z}\right)^2\right)\right)\left(1+\left(\frac{\partial S}{\partial z}\right)^2\right)^{-\frac{1}{2}} = 0, \tag{15}$$

where $J=\sigma\rho R_1/\mu_1^2$ is the non-dimensional surface tension parameter. The system is closed by imposition of a kinematic condition stating that the interface is a material surface,

$$U_j=\frac{\partial S}{\partial t}+W_j\frac{\partial S}{\partial z} \qquad \text{at } r=S(z,t). \tag{16}$$

3 The thin film limit

The full nonlinear problem (10), (11), (12), (13), (15) and (16) presents a formidable analytical and computational task even under the reasonable assumption that the flow is axisymmetric. Considerable progress can be made, however, in situations when the annulus is thin compared with the core and when capillary instability is important (see Introduction for the physical significance of such limits.) We proceed, then, by formulating the stability problem for oscillatory core-annular flow where the annular layer is thin, referring to this layer as the film. In this regime $a=1+\epsilon$ with $\epsilon \ll 1$ so that the film has thickness $O(\epsilon)$ and we introduce a strained local coordinate y given by

$$r=1+\epsilon(1-y). \tag{17}$$

The flow described by (10)-(16) is now regarded as a perturbation to the basic state $(\overline{\mathbf{U}}_{c,f}, \overline{P}_{c,f})$, where the subscripts c and f denote the core and film regions respectively. The unknown interface position is written as $r = S(z,t) = 1 + \delta\eta(z,t)$, with $\delta \ll \epsilon$ (in the absence of a shear flow δ can be as large as $O(\epsilon)$ and the analysis presented below is still applicable) and to be determined by the main asymptotic balances (see below). The velocity perturbation in each layer is denoted by $(\widetilde{U}, \widetilde{V}, \widetilde{W})_{c,f}$ and surface tension induces a jump in pressure $\widetilde{P}_{c,f}$ across the interface. The equation of normal stress indicates that this jump is of relative magnitude $J\delta R_e^{-2}$. The core and film dynamics are coupled by a balance of tangential stresses across the interface, and the relative asymptotic sizes of perturbed quantities in each layer then follow by balancing appropriate terms (see PMR also). It has been shown in PMR, and is also true for the present problem, that capillary forces affect the dynamics to leading order in the perturbation as long as the non-dimensional film depth, ϵ, the surface tension group J, and the core speed characterized by the Reynolds number R_e, satisfy the constraint $\epsilon J \sim R_e$. This is achieved by considering either of the following cases

A: slow core flow with moderate surface tension, $R_e \sim \epsilon$ and $J \sim 1$;

B: moderate core flow with large surface tension, $R_e \sim 1$ and $J \sim \epsilon^{-1}$.

To facilitate the balance of terms, a Taylor expansion about the unperturbed position $r = 1$ is used to describe the interface conditions. For example the undisturbed film velocity at the interface $\overline{W}_f(S(z,t))$ may be written as the sum of the steady and unsteady parts

$$\begin{aligned}
\overline{W}_f(r,t) &= \overline{W}_f^{(s)}(r) + \overline{W}_f^{(us)}(r,t), \\
\overline{W}_f^{(s)}(1+\delta\eta) &= \frac{2\epsilon}{m} + \frac{\epsilon^2}{m} - \frac{4\epsilon^2}{m^2} - \frac{2\delta\eta}{m} + O\left(\epsilon^3\right) + O(\epsilon\delta), \\
\overline{W}_f^{(us)}(1+\delta\eta,t) &= \Re\left\{\left[\frac{\delta\eta\beta I_1(\beta)}{mI_0(\beta)} - \frac{\beta}{mI_0(\beta)}\left(1 + \frac{\delta\eta\beta I_1(\beta)}{mI_0(\beta)}\right)(\epsilon I_1(\beta)\right.\right. \\
&\quad - \frac{\epsilon^2}{2}(I_1(\beta) - \beta I_0(\beta)) - \frac{\epsilon^2\beta I_1^2(\beta)}{mI_0(\beta)} + O\left(\epsilon^3\right)\Big) \\
&\quad + \left.\left. O(\epsilon\delta)\right]\frac{i\Delta}{\Omega R_e}\exp(i\Omega t)\right\},
\end{aligned}$$

and the kinematic condition (16) becomes

$$\widetilde{U}_f = \delta\frac{\partial\eta}{\partial t} + \delta\left(\overline{W}_f + \widetilde{W}_f\right)\frac{\partial\eta}{\partial z}, \qquad \text{at } r = 1 + \delta\eta. \tag{18}$$

It follows by leading order balances (see PMR for further details) that

$$\widetilde{U}_f \sim \epsilon^2\delta, \qquad \delta \sim \epsilon^2, \qquad \tau \sim \delta t,$$

where τ is the long time scale for the temporal instability. The oscillatory unsteady flow is of the form $\exp(i\Omega t)$, and in the analysis that follows we consider low frequency oscillations so that $\Omega t \sim 1$ with $\Omega = \epsilon^2\Omega_0$. Noting that

$$\begin{aligned}
\beta &= (1+i)\epsilon\left(\frac{\Omega_0 R_e}{2}\right)^{\frac{1}{2}}, \\
I_0(\beta) &= 1 + \frac{iR_e\epsilon^2\Omega_0}{4} + O\left(R_e^2\epsilon^4\right), \\
I_1(\beta) &= (1+i)\epsilon\left(\frac{R_e\Omega_0}{8}\right)^{\frac{1}{2}}\left[1 + \frac{iR_e\epsilon^2\Omega_0}{8} + O\left(R_e^2\epsilon^4\right)\right],
\end{aligned}$$

we transform the coordinate system to one which oscillates and moves down the core with speed $2\epsilon m^{-1} + O(\epsilon^2)$, by introducing the transformation

$$z \longrightarrow z - \left[\frac{2\epsilon}{m} + \frac{\epsilon^2}{m} - \frac{4\epsilon^2}{m^2} + O\left(\epsilon^3\right)\right] t - \left[\frac{\epsilon\Delta}{2m\Omega}(1+\epsilon) + O\left(\epsilon^3\right)\right] \sin(\Omega t). \tag{19}$$

With respect to this oscillating frame of reference the leading order kinematic condition reduces to

$$\epsilon^{-4}\widetilde{U}_f = \frac{\partial \eta}{\partial \tau} - \left(\frac{2}{m} + \frac{\Delta}{2m}\cos(\Omega_0 \tau)\right)\eta\frac{\partial \eta}{\partial z}. \tag{20}$$

An evolution equation for $\eta(z,t)$ follows from (20) once $\tilde{U}_f$ is expressed in terms of η. This is achivable by matching with the core dynamics as described next.

3.1 Slow flow, moderate surface tension

Consider first the case when $R_e \sim \epsilon$ and $J \sim 1$. The perturbation velocities in the film and core become

$$U_f = \widetilde{U}_f = \epsilon^4 U_{f0} + \ldots, \tag{21a}$$
$$W_f = \overline{W}_f + \widetilde{W}_f = \overline{W}_f + \epsilon^3 W_{f0} + \ldots, \tag{21b}$$
$$P_f = \overline{P}_f + \widetilde{P}_f = \overline{P}_f + \epsilon P_{f0} + \ldots, \tag{21c}$$

$$U_c = \widetilde{U}_c = \epsilon^2 U_{c0} + \ldots, \tag{22a}$$
$$W_c = \overline{W}_c + \widetilde{W}_c = \overline{W}_c + \epsilon^2 W_{c0} + \ldots, \tag{22b}$$
$$P_c = \overline{P}_c + \widetilde{P}_c = \overline{P}_c + \epsilon P_{c0} + \ldots, \tag{22c}$$

and $R_e = \lambda\epsilon$ and $\lambda = O(1)$. Substitution of (21a-c) into (12)-(14) along with the local film scaling (17) yields the following leading order solutions in the film,

$$P_{f0} = P_{f0}(z,\tau), \tag{23}$$
$$W_{f0} = \frac{\lambda}{m}\left[\frac{y^2}{2}\frac{\partial(P_{f0})}{\partial z} + yA(z,\tau)\right], \tag{24}$$
$$U_{f0} = \frac{\lambda}{m}\left[\frac{y^3}{6}\frac{\partial^2(P_{f0})}{\partial z^2} + \frac{y^2}{2}\frac{\partial A}{\partial z}\right]. \tag{25}$$

The solution in the core is found in Fourier space and couples with the film through the balance in tangential stress to determine the function $A(z,\tau)$.

$$-m\frac{\partial W_{f0}}{\partial y}(1) = \frac{\partial U_{c0}}{\partial z}(1) + \frac{\partial W_{c0}}{\partial r}(1). \tag{26}$$

Substitution of (22a-c) into (10), (11) and (14) gives the following leading order core problem

$$\nabla^2 U_{c0} - \frac{U_{c0}}{r^2} = \lambda\frac{\partial P_{c0}}{\partial r}, \tag{27a}$$
$$\nabla^2 W_{c0} = \lambda\frac{\partial P_{c0}}{\partial z}, \tag{27b}$$
$$\frac{\partial(rU_{c0})}{\partial r} + \frac{\partial W_{c0}}{\partial z} = 0. \tag{27c}$$

which is to be solved subject to the continuity of velocity conditions

$$\begin{aligned} U_{c0}(r=1) &= 0, \\ W_{c0}(r=1) &= 2\eta\left(\frac{m-1}{m}\right). \end{aligned}$$

Defining a streamfunction ψ in the usual way, $U_{c0} = -\frac{1}{r}\frac{\partial \psi}{\partial z}$, $W_{c0} = \frac{1}{r}\frac{\partial \psi}{\partial r}$, the system (27a-c) yields the familiar Stokes operator for ψ,

$$\left(\frac{\partial^2}{\partial r^2} - \frac{1}{r}\frac{\partial}{\partial r} + \frac{\partial^2}{\partial z^2}\right)^2 \psi = 0,$$

with solution readily obtainable in Fourier space in terms of modified Bessel functions

$$\begin{aligned} \widehat{\psi} &= \int_{-\infty}^{\infty} \psi(r,z)\, e^{-ikz} dz, \\ \widehat{\psi} &= -rI_0(k)\, F(k)\, \widehat{\eta} I_1(kr) + r^2 I_1(k)\, F(k)\, \widehat{\eta} I_0(kr), \qquad (28) \\ F(k) &= \frac{2(m-1)}{m\left[kI_1^2(k) - kI_0^2(k) + 2I_0(k)\, I_1(k)\right]}. \end{aligned}$$

The leading order radial velocity perturbation in the film is then evaluated at $y = 1$ and on elimination of $A(z,t)$ from (23)-(25), (26) and (28) can be written in the form

$$\widehat{U}_{f0}(1) = -\frac{2i}{m}\left(1 - \frac{1}{m}\right) N(k)\, \hat{\eta} + \frac{\lambda}{3m} k^2 \widehat{P}_{f0}, \qquad (29)$$

where the the kernel $N(k)$ is given by

$$N(k) = \frac{k^2 I_1^2(k)}{\left[kI_1^2(k) - kI_0^2(k) + 2kI_0(k)\, I_1(k)\right]}. \qquad (30)$$

¿From the kinematic condition (18) and continuity of normal stresses (15) respectively, we have

$$\begin{aligned} U_{f0}(y=1) &= \frac{\partial \eta}{\partial \tau} - \left(\frac{2}{m} + \frac{\Delta}{2m}\cos(\Omega_0 \tau)\right)\eta \frac{\partial \eta}{\partial z}, \qquad (31) \\ P_{f0} &= \frac{J}{\lambda^2}\left(\eta + \frac{\partial^2 \eta}{\partial z^2}\right), \end{aligned}$$

and substituting (29) into (31) yields the desired evolution equation

$$\begin{aligned} &\frac{\partial \eta}{\partial \tau} - \left(\frac{2}{m} + \frac{\Delta}{2m}\cos(\Omega_0 \tau)\right)\eta \frac{\partial \eta}{\partial z} + \frac{J}{3m\lambda}\left(\frac{\partial^2 \eta}{\partial z^2} + \frac{\partial^4 \eta}{\partial z^4}\right) + \\ &\frac{i(m-1)}{\pi m^2}\int_{-\infty}^{+\infty}\int_{-\infty}^{+\infty} N(k)\, \eta(z_1,\tau) \exp\left(ik(z-z_1)\right) dz_1\, dk = 0. \qquad (32) \end{aligned}$$

It should be noted that (32) is a long-wave equation since it has been derived by assuming that the radial lengthscales in the film are much smaller than the axial ones. The validity of this assumption is checked *a posteriori* by studying the solutions of (32) and showing that no infinite slope singularities will arise. This has been proven for the KS equation analytically (see Introduction for references) and we provide evidence that this is also true for (32) from our extensive numerical work (see later).

3.2 Moderate flow, large surface tension

The analysis presented in the previous Section applies also, with minor modifications when $R_e \sim 1$ and $J \sim \frac{1}{\epsilon}$. For brevity we present the essential differences and refer the reader to PMR for a complete derivation. The dynamics in the film as well as the asymptotic solution there has the same form as above. Coupling between film and core is still achieved through the tangential stress balance and the normal stress balnace yields a pressure jump as before. The main difference is in the core dynamics: Since the Reynolds number is $O(1)$ now, the equations governing the perturbation there are the linearized *steady* Navier-Stokes equations (see PMR). The perturbation equations apear steady by virtue of the time-scale of the evolution. In particular, the core variables expand as

$$U_c = \epsilon^2 U_0 + \ldots, \tag{33a}$$

$$W_c = \overline{W}_c + \epsilon^2 W_0 + \ldots, \tag{33b}$$

$$P_c = \overline{P}_c + \epsilon^2 P_0 + \ldots. \tag{33c}$$

The time-scale transforms according to the change of reference frame given by (19) and substitution of this along with (33a-c) into the core Navier-Stokes equations (10)-(11) together with the intrduction of the streamfunction ψ defined in Section 3.1, yields

$$(1-r^2)\frac{\partial}{\partial z}(D\psi) = \frac{1}{R_e} D^2\psi, \tag{34}$$

$$D = \left(\frac{\partial}{\partial}\partial r^2 - \frac{1}{r}\frac{\partial}{\partial r} + \frac{\partial^2}{\partial z^2}\right). \tag{35}$$

Solution of (34) is achieved by taking the fourier transform in z and the final evolution equation is obtained after satisfaction of all the boundary conditions (see PMR also). The result is

$$\frac{\partial \eta}{\partial \tau} - \left(\frac{2}{m} + \frac{\Delta}{2m}\cos(\Omega_0 \tau)\right)\eta\frac{\partial \eta}{\partial z} + \frac{J}{3m\lambda}\left(\frac{\partial^2 \eta}{\partial z^2} + \frac{\partial^4 \eta}{\partial z^4}\right) -$$

$$\frac{i(m-1)}{2\pi m}\int_{-\infty}^{+\infty}\int_{-\infty}^{+\infty} N(k)\,\eta(z_1,\tau)\exp(ik(z-z_1))\,dz_1\,dk = 0. \tag{36}$$

The kernel $N(k)$ appearing above is expressible in terms of the confluent hypergeometric function and two auxiliary integrals given below,

$$\begin{aligned} N(k) &= \frac{I_1(k)e^{-\lambda}M(\Lambda,2,2\lambda)}{N_1(k)I_0(k) - N_2(k)I_1(k)}, \\ N_1(k) &= \int_0^1 (I_1(k)K_1(ks) - I_1(ks)K_1(k))s^2 e^{-\lambda s^2} M(\Lambda,2,2\lambda s^2)ds, \\ N_2(k) &= \int_0^1 (I_0(k)K_1(ks) + I_1(ks)K_0(k))s^2 e^{-\lambda s^2} M(\Lambda,2,2\lambda s^2)ds, \end{aligned} \tag{37}$$

where $\lambda = \frac{1}{2}(kR_e)^{\frac{1}{2}}e^{-\frac{i\pi}{4}}$ and $\Lambda = 1 + \frac{k^2}{8\lambda} - \frac{\lambda}{2}$, while M is the regular solution of the equation

$$\xi G'' + (2-\xi)G' - \Lambda G = 0, \tag{38}$$

with primes denoting ξ-derivatives. Note that in order to solve (36) the kernel $N(k)$ need only be computed once, given a value of ν. This was done, in the absence of background fluctuations, by

PMR where it is shown numerically that the effect of the kernel (physically this is the viscosity stratification mechanism) is to organize the evolution into travelling waves for a wide range of parameters.

4 Analysis of the evolution equations

The time evolution of the interface position η is described by equations (32) and (36). The following change of variables yields the canonical equation (39) given below

$$\tau = \frac{3m\lambda t_1}{J\nu}, \quad \eta = -\frac{\nu^{\frac{1}{2}} J}{6\lambda} u, \quad z = \nu^{-\frac{1}{2}} x, \quad \nu = \frac{\pi^2}{L^2}, \quad k = \nu^{\frac{1}{2}} k',$$

where L is the unscaled wavelength of the interface.

$$\frac{\partial u}{\partial t} + (1 + \delta_1 \cos(\omega_1 t)) u \frac{\partial u}{\partial x} + \frac{\partial^2 u}{\partial x^2} + \nu \frac{\partial^4 u}{\partial x^4} + i \left(\frac{m-1}{m} \right) \mathcal{L}(u) = 0, \tag{39}$$

where

$$\begin{aligned} \delta_1 &= \frac{m^2 \Delta}{4}, \\ \omega_1 &= \frac{3m\lambda\Omega_0}{J\nu}, \\ \mathcal{L}(u) &= \frac{3\lambda}{\pi J \nu} \int_{-\infty}^{\infty} \int_{-\infty}^{\infty} N\left(\nu^{\frac{1}{2}} k\right) u(x_1, t) e^{ik(x-x_1)} dx_1 dk. \end{aligned}$$

According to the change of variables above, we choose to construct solutions of equation (39) on spatially periodic domains; in physical space the limit $\nu \to 0$ corresponds to $L \to \infty$.

We begin to analyze the nonlinear dynamics of oscillatory CAFs by studying the oscillatory KS equation (referred to hereafter as the OSCKS equation). This limit corresponds to the nonlocal term in equation (39) being absent and is relevant if the viscosities of the two fluids are the same ($m = 1$) or if the Reynolds number is small for example of order ϵ^2 or smaller (for a justification of the latter limit see [[8]]). The oscillatory KS equation (OSCKS) and the KS equation share the same linear stability spectrum when linearization is done about $u = 0$. More importantly $\int_0^{2\pi} u(t,x)dx$ is a conserved quantity for both equations along with the fact that the energy equation for the evolution of $\int_0^{2\pi} u^2 dx$ is the same (this equation is easily obtained by multiplying (39) by u and integrating). As a result of this it can be concluded that when $\nu > 1$ solutions will tend to a uniform steady state and nontrivial dynamics first enter when ν crosses below unity and linearly unstable modes are activated.

The main purpose of this Section is to gain an understanding of the dynamics of the OSCKS equation. Due to the nonlinear nature of the problem we undertake extensive numerical work, but before presenting such results we consider the limit $\nu \to 1-$ which can be described analytically.

4.1 Asymptotic solutions of the OSCKS equation for ν near 1

As mentioned above, when $\nu > 1$ there are no linearly unstable modes to pump energy into the system and if the initial condition has zero mean then the large time evolution yields a trivial steady state. ¿From a normal mode linear stability analysis of the OSCKS equation (equation (39) with $m = 1$), it is clear that that the number of linearly unstable modes is mod $[\nu^{-\frac{1}{2}}]$ and by setting

$$\nu = 1 - \epsilon_1, \qquad 0 < \epsilon_1 << 1,$$

we are in a position to study the evolution in the neighborhood of the first unstable mode. In what follows we begin by consideration of solutions with zero mean and odd parity. We note that for ν near 1 (but not necessarily asymptotically close), the KS has a global steady state attractor which can be cast into an odd-parity zero-mean profile by Galilean transformation and translation invariance. Using Fourier analysis, then, we can represent zero mean odd-parity solutions by the infinite sum

$$u(x,t) = \sum_{k=1}^{\infty} a_k(t)\sin(kx). \tag{40}$$

The partial differential equation is dissipative and we expect a low modal behavior as for the KS equation. In practice this means that a Galerkin approximation can be employed to truncate the sum in (40) to N terms, with N depending on ν and also on δ_1. ¿From previous work on the KS (see PS and SP) we find that a few modes more than the number of linearly unstable ones provide a sufficient description of the attractors. In the analysis that follows the asymptotic limit $\epsilon_1 \to 0$ is described by the two leading modes a_1 and a_2. The equations satisfied by a_1 and a_2 are

$$\frac{da_1}{dt} - (1+\delta_1\cos(\omega_1 t))\frac{a_1 a_2}{2} - \epsilon_1 a_1 = 0, \tag{41a}$$

$$\frac{da_2}{dt} + (1+\delta_1\cos(\omega_1 t))\frac{a_1^2}{2} + (12-16\epsilon_1)a_2 = 0. \tag{41b}$$

This is a two-dimensional dynamical system and our main concern is with the behavior at large times which provides the features of the attractor for this range of values of ν. In the context of the Galerkin approximation the system (41a-b) is exact; its validity hinges on the fact that there are only two modes of importance, something which can be true if ν is near 1 and ϵ_1 is small. In practice ϵ_1 need not be asymptotically small for the two-mode truncation to be a reasonable approximation; this is shown later (see Figure 2) by a computation with $\epsilon_1 = 0.1$ and with 2 modes or 20 modes respectively with indistinguishable results. The smallness of ϵ_1 can be used, however, in an analytical description of these solutions and consequently provide an accurate description of the dynamics.

In order to motivate the multiple scales ansatz to follow, we consider first the solution of (41a-b) when $\delta_1 = 0$. If the unsteady terms are dropped the steady states are obtained by solution of two coupled algebraic equations which yield $a_1 = \sqrt{48\epsilon_1}$ and $a_2 = -2\epsilon_1$. There does not appear to be a closed form solution for a_1 and a_2 at general times but a multiple scales analysis can be used to provide the essential features of the dynamics. It can be seen that since $a_1 \sim \sqrt{\epsilon_1}$ and $a_2 \sim \epsilon_1$, the principal time scale is long and of order ϵ_1^{-1}. With δ_1 non-zero (and ω_1 of order 1 or smaller) the appropriate expansion is

$$a_1(t) = \epsilon_1^{1/2}\left[A_{10}(t_1,t_2,\ldots) + \epsilon_1 A_{11}(t_1,t_2,\ldots) + \ldots\right], \tag{42a}$$

$$a_2(t) = \epsilon_1\left[A_{20}(t_1,t_2,\ldots) + \epsilon_1 A_{21}(t_1,t_2,\ldots) + \ldots\right], \tag{42b}$$

where the multiple scales are given by

$$t_1 = t, \quad t_2 = \epsilon_1 t, \quad t_3 = \epsilon_1^2 t, \quad \ldots \ .$$

Substitution of (42a-b) into (41a-b) yields the following equations to leading order

$$\frac{\partial A_{10}}{\partial t_1} = 0, \tag{43}$$

$$\frac{\partial A_{11}}{\partial t_1} + \frac{\partial A_{10}}{\partial t_2} - \frac{1}{2}(1 + \delta_1 \cos(\omega_1 t_1))A_{10}A_{20} - A_{10} = 0, \tag{44}$$

$$\frac{\partial A_{20}}{\partial t_1} + \frac{1}{2}(1 + \delta_1 \cos(\omega_1 t_1))A_{10}^2 + 12A_{20} = 0, \tag{45}$$

$$\frac{\partial A_{21}}{\partial t_1} + \frac{\partial A_{20}}{\partial t_2} + (1 + \delta_1 \cos(\omega_1 t_1))A_{10}A_{11} + 12A_{21} - 16A_{20} = 0. \tag{46}$$

It can be seen from (43) that A_{10} is independent of t_1 and it follows from (45) that

$$A_{20} = K_1 e^{-12t_1} - A_{10}^2 \left(6\gamma \cos(\omega_1 t_1) + \frac{1}{2}\gamma\omega_1 \sin(\omega_1 t_1) + \frac{1}{24}\right), \tag{47}$$

where

$$\gamma = \frac{\delta_1}{144 + \omega_1^2}.$$

The value of K_1 in (47) is fixed by the initial conditions and does not affect the large time behavior of the solutions. With A_{20} available, then, we turn to (44). Since A_{10} is independent of t_1, solutions of (44) will become unbounded as t_1 increases unless a secularity condition is satisfied. This arises by setting to zero terms in the forcing function which do not involve t_1; this is shown explicitly below by a re-grouping of terms in (44).

$$\frac{\partial A_{11}}{\partial t_1} - \frac{1}{2}A_{10}\left[Ke^{-12t_1}(1 + \delta_1 \cos(\omega_1 t_1)) - (6\gamma + \frac{\delta_1}{24})A_{10}^2 \cos(\omega_1 t_1)\right.$$
$$\left. -\frac{1}{2}\omega_1\gamma A_{10}^2 \sin(\omega_1 t_1) - 3\gamma\delta_1 A_{10}^2 \cos(2\omega_1 t_1) - \frac{1}{4}\omega_1\gamma\delta_1 A_{10}^2 \sin(2\omega_1 t_1)\right]$$
$$+\frac{\partial A_{10}}{\partial t_2} + \alpha^2 A_{10}^3 - A_{10} = 0,$$

where

$$\alpha^2 = \left(\frac{1}{48} + \frac{3\gamma\delta_1}{2}\right).$$

The secularity condition is, then,

$$\frac{\partial A_{10}}{\partial t_2} + \alpha^2 A_{10}^3 - A_{10} = 0,$$

which gives the following explicit solution for A_{10},

$$A_{10}^2 = \frac{K_2}{\alpha^2 L + e^{-2t_2}},$$

where K_2 is fixed by the initial conditions. With A_{10} and A_{20} known, higher order terms can be calculated by direct integration and application of secularity conditions where necessary.

Of particular interest is the comparison between the asymptotic solutions just described and the numerical solutions of (41a-b) for small ϵ_1. For large times the leading order solutions are

$$A_{10} \sim \left(\frac{1}{48} + \frac{3\delta_1^2}{2(144 + \omega_1^2)}\right)^{-\frac{1}{2}}, \tag{48a}$$

$$A_{11} \sim \frac{1}{2\alpha^3}\left[-\left(\frac{6\gamma}{\omega_1} + \frac{\delta_1}{24\omega_1}\right)\sin(\omega_1 t_1) + \frac{\gamma}{2}\cos(\omega_1 t_1)\right. \tag{48b}$$

$$\left. - \frac{3\gamma\delta_1}{2\omega_1}\sin(2\omega_1 t_1) + \frac{\gamma\delta_1}{8}\cos(2\omega_1 t_1)\right], \tag{49b}$$

$$A_{20} \sim -\left(\frac{1}{48} + \frac{3\delta_1^2}{2(144 + \omega_1^2)}\right)^{-1}\left(6\gamma \cos(\omega_1 t_1) + \frac{1}{2}\omega_1\gamma \sin(\omega_1 t_1) + \frac{1}{24}\right). \tag{49c}$$

It is seen from (48a-c) that the leading order solution A_{10} of a_1 is a constant while the next order correction, namely A_{11}, provides an oscillatory component of period $2\pi/\omega_1$. For the Fourier mode a_2 the oscillations are captured at leading order by the asymptotic expression A_{20} the period being $2\pi/\omega_1$. These analytical results suggest, therefore, that the effect of the oscillatory pressure gradient in the undisturbed flow is to induce a nonlinear interfacial evolution (within the framework of the present work) which is (i) spatially periodic with wavelength $2\pi\nu^{-\frac{1}{2}}$ with ν slightly less than unity, and, (ii) which is time-periodic with frequency locked to that of the driving pressure gradient. Such behavior is also seen in related two-dimensional systems such as the forced Duffing oscillator for instance (see Chow & Hale (1982) for example). The forcing in the present problem is different in that it only alters the distribution of energy rather than adding or removing energy from the system. The evolution of the OSCKS becomes increasingly complicated as ν decreases and the dimension of the attractors increases; in the following Section we carry out extensive numerical experiments in order to gain an understanding of the attractors for this system.

Before presenting direct numerical simulations of the OSCKS, we provide a comparison between the multiple scales asymptotic theory and the numerical solution of (41a-b). The important parameter is ϵ_1 and numerical results with different values of ω_1 and δ_1 are qualitatively similar; in what follows, therefore, we fix the values $\omega_1 = 1$ and $\delta_1 = 0.5$ and carry out an evaluation of the asymptotic theory for a range of ϵ_1. Equations (41a-b) were integrated numerically by specifying initial conditions $a_1 = 1$, $a_2 = 0$ at time $t = 0$ and solving to large enough times so that any transient behavior disappears. The Fourier component a_1 is compared with the corresponding two-term asymptotic solution $\epsilon_1^{\frac{1}{2}} A_{10} + \epsilon_1^{\frac{3}{2}} A_{11}$, while the second Fourier component a_2 is compared with its corresponding one-term asymptotic solution $\epsilon_1 A_{20}$. Numerical solutions are given in Figure 1 for values of $\epsilon_1 = 0.1$ and $\epsilon_1 = 0.01$. The agreement is seen to be very good with additional improvement as ϵ_1 decreases. By analyzing the phase plane of the energy, we have verified that the solutions are indeed periodic and frequency-locked to the background flow oscillations, with a period of 2π for both cases. The fact that the two-mode truncation is a very good approximation to the solution is illustrated in Figure 2. A numerical solution has been obtained using 20 modes (see the next section for details) and a comparison is made between the Fourier coefficients a_1 and a_2 as well as the corresponding asymptotic expressions. The dotted lines correspond to the asymptotic results and it is seen that the 2 mode and 20 mode truncations produce almost identical results.

5 Numerical experiments on the OSCKS

The solution of the full nonlinear evolution equation (39) for general values of ν, δ_1 and ω_1 must in general be obtained numerically. The method we apply here is an adaptation of the scheme developed by PS and SP for the solution of the KS equation, which is obtainable from (39) when $m = 1$ and $\delta_1 = 0$.

5.1 Numerical methods

The following Galerkin approximation is used to approximate solutions with zero mean

$$u(t,x) = \sum_{k=1}^{N} \left(a_k(t) \sin(kx) + b_k(t) \cos(kx) \right). \tag{50}$$

When $m \neq 1$ the solution contains both sines and cosines whereas when $m = 1$ the symmetry of (39) allows odd-parity solutions for which $b_k = 0$ in (50). Such odd-parity solutions would evolve from odd-parity initial data for instance; general initial conditions, however, require both sines and

cosines and so there are twice as many unknowns then. Briefly, then, when (50) is substituted into (39) and coefficients of the different harmonics are set to zero, a nonlinear system of $2N$ (or N) coupled first order differential equations are obtained for the evolution of the fourier coefficients (see PS). These equations when written as a first order system, contain a nonlinear coupling term and a linear term resulting from the fourier projection of the linear spatial operators in (39). A split-step scheme is implemented with the linear part (which contains all the stiffness at large N and the dispersive effects due to the pseudo-differential operator) integrated exactly and the nonlinear part with a fourth order variable step Runge-Kutta method. Accuracy tests are applied at each time-step. For particular experiments the number N is chosen large enough so that the minimum amplitude of any of the fourier components is below a tolerance level (this tolerance is usually set to $< 10^{-8}$). The linear dispersive term also imposes a restriction on the time-step as we explain next with the model $u_t + u_{xxx} = 0$: The solution of the kth fourier coefficient after a time-step Δt is proportional to $\exp(ik^3\Delta t)$; the exponential is evaluated accurately, then, if $k_{max}^3 \Delta t \ll 1$. In practice we allowed the upper bound to be about $0.1 - 0.3$ without loss of accuracy. All numerical experiments described below and which contain high frequency oscillations superimposed onto the lower frequency background flow have been confirmed by convergence studies in both N as well as the time-step.

In the presence of periodic forcing ($\delta_1 \neq 0$) solutions of equation (39) display a variety of interesting behavior as ν decreases below 1. For various values of ω_1 and δ_1 we have characterized the effect of the oscillations on a number of attractors. In Table 1 we provide some representative behavior for odd-parity solutions generated by the initial condition $u(0,x) = -\sin(x)$; these results are discussed in Section 5.2 below. General initial conditions were also used to compute asymmetric profiles; in many instances the initial conditions are taken to be random and so the attractors we compute and describe below in Section 5.3 and Table 2 are those with the largest basin of attraction. In Section 5.4 we give some results for $m \neq 1$ and in particular try to quantify the effect of large dispersion on the dynamics. We use various diagnostic tools to analyze the data of our numerical experiments and use them to infer the type of attractors present. These techniques are summarized in the Appendix.

5.2 Odd parity solutions of the OSCKS

When $\delta_1 = 0$, odd-parity solutions of the KS equation for $1 > \nu \geq 0.06$ (approximately) are attracted to a non-uniform steady state. Within this window, are sub-windows where fully modal, bimodal and trimodal attractors are observed, with respective spatial periods of 2π, π, and $3\pi/2$. For $\delta \neq 0$ and for $1 > \nu \geq .06$ our numerical experiments show that solutions of the OSCKS equation lock into the frequency of the forcing pressure gradient $\delta_1 \cos(\omega_1 t)$.

For example, the attractor of the odd-parity KS at $\nu = 0.1$ yields a bi-modal steady state which becomes time-periodic when $\delta_1 \neq 0$. The time dependence is seen in Figure 3a where the evolution of the energy of the solution, $E(t) = \frac{1}{2\pi}\int_0^{2\pi} u^2(t,x)dx$ say, is plotted for two different frequencies, $\omega_1 = 1, 2$. It is found that $E(t)$ is periodic of period $\frac{2\pi}{\omega_1}$. The spatial characteristics of the flow are preserved by the forcing as shown Figure 3b. This picture was produced as follows: If the flow is periodic in t, then $u(t,x) = u(t + \frac{2\pi}{\omega_1}, x)$ and so plotting $u(t,x)$ at time intervals separated by $\frac{2\pi}{\omega_1}$ should yield the same curve as seen in Figure 3b. Further more we chose to plot u at times in its cycle where $E(t)$ is maximum and $u_x(t,0) > 0$ and compared the profile with the steady-state solution of the KS for $\delta_1 = 0$, finding identical results. It can be concluded, therefore, that the forcing in this case produces a standing wave locked onto the driving pressure gradient.

The KS equation also supports windows in the parameter space (ν) where chaos is preceded by a complete sequence of period doubling bifurcations (see SP and PS). One particular example is

the case $\nu = 0.0303$ for which the period is 0.89 time units. The behavior of this attractor in the presence of harmonic background forcing was analyzed by following the evolution of u for various values of δ_1 and ω_1. Even for small δ_1 the periodic attractor is found to become quasi-periodic after a long time. Figures 4(a-c) show $E(t)$, the phase plane of $E(t)$ and the return map of the minima, for increasing $\delta_1 = 0.01, 0.1, 0.5$ respectively, and fixed forcing frequency $\omega_1 = 1.0$. As δ_1 increases from 0.01 to 0.1, it is seen from Figures 4(a) and 4(b) that the energy has two dominant time scales: an oscillation with period roughly that of the KS with $\delta_1 = 0$ and a longer modulation with period roughly 2π provided by the forcing pressure gradient. The interaction between the two frequencies produces a quasi-periodic flow as can be seen from the return maps in Figures 4(a),(b) which are two closed unfolded loops in both cases. One of the loops in Figure 4(a) is very flat and appears as a line but an enlargement shows an open loop. The phase-plane is more revealing for the $\delta_1 = 0.01$ case; the lower modulational frequency is responsible for the larger turns while the higher frequency produces the smaller turns in the phase-plane. The spacings between turns eventually fill out more and more indicating the quasi-periodicity confirmed numerically by the return maps. When δ_1 is increased further to a value of 0.5, it is found that after approximately 160 time units of irregular modulated high frequency oscillations the solution locks into the forcing frequency and its period is 2π. This is confirmed further by the phase-plane and the return map which contains only a single point - see Appendix.

For $\nu \ll 1$ we observe regions of chaotic oscillations for the solution of both the KS equation and the OSCKS equation. The aperiodic oscillations alternate with periodic/quasi-periodic regions, but the lengths of the subwindows become vanishingly small as ν decreases. A phase-plane analysis and the return map of the minima do not indicate recognizable behaviour, such as strange attractors.

5.3 Solutions of the OSCKS equation with general initial data

We have also computed a number of solutions of (39) for general initial data. These computations are more expensive that those of Section 5.2 since there are twice as many equations now. This class of solutions gives richer dynamics for both the KS and OSCKS equations. For the KS equation, for example, we observe various steady state attractors for a wide range of $\nu < 1$, but in addition, additional dynamics are found such as travelling waves and homoclinic bursting (periodic and aperiodic). Consider for example the case $\nu = 0.3$ for which the KS equation yields a travelling wave solution. Figure 5(a) shows that the energy quickly evolves to a constant value (4.27 approximately) and a steady-state travelling wave emerges after a long time whose phase-speed is small but non-zero. The travelling wave can be seen from the last figure which was produced by recording the solution after 11 equal time intervals and shifting each profile verically by 5 units. Figures 5(b),(c) show the effect of the background oscillations on the steady-state travelling wave depicted in Figure 5(a). The values of δ_1 are 0.01 and 0.1 respectively and the OSCKS equation is found to yield a wave which oscillates quasi-periodically and also travels. The return maps indicate that the solution is quasi-periodic.

In the window $0.23249 > \nu > 0.17735$ solutions of the KS equation undergo periodic homoclinic bursting. A representative case has $\nu = 0.22$ and is depicted in Figure 6(a) which shows that the energy remains constant for approximately 21 time units between each localized burst. The phenomenon is time periodic and repeats itself as indicated by the phase plane which contains about 20 turns (for the developed solution) superimposed on each other. Even for a small $\delta = 0.05$, the solution of OSCKS equation appears to be chaotic even after a significant time has elapsed. The phase plane analysis and the return map do not give convincing evidence of quasi-periodicity. It is interesting to note from the return map that the solution is almost quasi-periodic but drifts away from the what would have been closed loops.

For smaller ν, solutions of both the KS and OSCKS equations show mostly chaotic oscillations. We present a typical case for the KS with $\nu = 0.1212$; the time history of $E(t)$ is chaotic but the phase plane is not sufficient to determine the type of oscillations present. The return map in Figure 7(a), however, indicates the presence of a strange attractor made up of five branches joined in a common region where folding takes place. Figure 7(aa) presents graphical evidence that the strange attractor is self-similar, by carrying out successive enlargements of the original return map; the dimensions of the first picture are 0.12×0.12 and by the fifth enlargement the size is 0.0001×0.0001 so that an enlargement of 1200 has taken place with the self-similarity clearly apparent. In the results presented in Figure 7(b) we quantify the effect of a background oscillation with $\delta_1 = 0.1$ on the chaotic motion of Figure 7(a). It can be seen that $E(t)$ is highly irregular and its phase plane yields a picture confirming this. The return map fails to produce a recognizable pattern; in fact from the return map we can exclude the possibilities of either quasi-periodic motion or chaotic motion with a strange attractor similar to the $\delta_1 = 0$ solution. It is possible that a strange attractor in a higher dimension than the plane is present (such a possiblity could be studied by forming the return map of triplets etc.) but this is not explored here.

5.4 Effects of viscosity stratification, $(m \neq 1)$

When the viscosities of the film and core fluids differ, a non local term $L(u)$ is introduced into the evolution equation (see (39). In the absence of oscillatory modulations in the driving pressure gradient, it has been shown in PMR that even for relatively small viscosity stratification (i.e. for m near 1), otherwise chaotic solutions of the equation describing the interfacial position (given by numerical solution of the KS equation), are organized into regular travelling wave pulses. This is true for both the canonical regimes presented in Sections 3.1 and 3.2 respectively. Physically this reflects the effect of dispersion provided by the viscosity stratification on the nonlinear waves; it has been established numerically for a wide range of ν that for $\delta_1 = 0$ there exists a critical value of m (which depends on ν) above which travelling waves are attained. The capillary terms (second and fourth derivatives) act to set the scale of the pulses which have been found to increase inamplitude as the dispersion increases. A detailed study of dispersive effects in core-annular flows can be found in Coward, Papageorgiou & Smyrlis (1994). To illustrate these results we present a numerical solution with the purely disspersive Bessel functions kernel of Section 3.1 at a value of $\nu = 0.1212$ and $\delta_1 = 0$ which for $m = 1$ yields chaotic oscillations (see Figure 7a). For $m = 3.0$ the large time evolution is attracted to a travelling wave state as shown in Figure 8 which depicts the time evolution over 4.5 spatial periods, by plotting the profiles at successive equispaced times by shifting them vertically by a small amount to facilitate the graphical representation.

A forced oscillation is now imposed on the flow of Figure 8 with a $\delta = 0.1$. The results are given in Figure 9: From the energy plot we see that a small oscillation persists about a constant value. This oscillation is brought out more clearly in the phase plane plot which indicates high frequency oscillations modulated by a low frequency motion provided by the forcing. A convergence study was done to verify that the high frequency oscillations are present and not due to numerical errors. In fact the modulated high frequency response is shown to be quasi-periodic by the return map of the energy minima shown in the last of Figure 9. The nonlinear travelling wave in the absence of forcing, then, is found to still preserve its travelling character as expected but also oscillates in time quasi-periodically. A picture of the wave motion is provided in Figure 10 which was produced in the same way as Figure 8 with a vertical shift of 3 units. The travelling component of the wave is easily discerned; the quasi-periodic modulations cause the small displacements in the wave and consequently the dark lines which are an indication of the locus of the wave minima in the $x - u$

plane are not straight lines but modulated around a straight line. An observation which is clearly illustrated by the spatial solution of Figure 10 in which u is given at successive time intervals, with

6 Conclusions

A weakly nonlinear asymptotic theory has been used to derive some novel partial differential equations that govern the stability of two-phase core-annular flow when an oscillatory pressure gradient acts. The equations extend the familiar Kuramoto-Sivashinsky models of CAFs to analogous evolution systems with time periodic coefficients. The main interest of this work is in the study of interfacial instability of oscillatory two-phase flows and the parametric evaluation of its effects on conventional CAF caused by constant pressure gradients. Such studies are desirable in the determination of physical mechanisms in complicated fluid flows which may be used advantageously to control inherent instabilities.

The main findings of our numerical experiments can be summarized in the following categories: (i) Stationary steady-states become time-periodic with frequencies locked to that of the forcing; (ii) Time periodic states become quasi-periodic,chaotic or lock into the forcing frequency if the forcing amplitude is large enough (for odd-parity solutions at least). (iii) Travelling wave states bacome travelling quasi-periodic waves. (iv) Periodic homoclinic bursts become unrecognized chaotic states. (v) Chaotic states which possess self-similar strange attractors become unrecognized chaotic states.

The forcing appears to promote irregular oscillations in regimes with large dispersion which would otherwise produce travelling wave pulses in unforced flows. The solutions in this case are perturbed by a quasi-periodic in time modulation whose amplitude increases with the forcing amplitude.

Our numerical results have not revealed any situations where the solutions lock into subharmonic or other lower frequencies with respect to the background forcing oscillation. It appears that if there is frequency locking this is at the driving frequency, for a wide range of parameters.

References

[1] Chen, K., Bai, R. & Joseph, D.D. 1990 Lubricated pipelining. Part 3. Stability of core-annular flow in vertical pipes. *J. Fluid Mech.* **214**, *251-286.*

[2] Chow, S.-N. & Hale, J.K. Methods of Bifurcation Theory, Springer- Verlag, New York, 1982.

[3] Constantin, P., Foias, C., Nicolaenko, B., Temam, R., *Integral Manifolds and Inertial Manifolds for Dissipative Partial Differential Equations*, Appl. Math. Sciences, No. 70, Springer-Verlag, New York, 1988.

[4] Coward, A.V. & Hall, P. 1993 On the nonlinear interfacial instability of rotating core-annular flow. *Theoret. Comput. Fluid Dynamics,* **5**, *269-289.*

[5] Coward, A.V. & Papageorgiou, D.T. 1994 Stability of oscillatory two-phase Couette flow. *IMA J. Appl. Maths, in the press.*

[6] Devaney, R.L., *An Introduction to Chaotic Dynamical Systems*, Benjamin/Cummings, Menlo Park, Ca., 1986.

[7] Feigenbaum, M. 1980 The transition to aperiodic behavior in turbulent systems, *Commun. Math. Phys.* **77**, *65-86.*

[8] Georgiou, E., Maldarelli, C., Papageorgiou, D.T. & Rumschitzki, D.S. 1992 An asymptotic theory for the linear stability of core-annular flow in the thin annular limit. *J. Fluid Mech.* **243**, *653-677.*

[9] Goren, S.L. 1962 The instability of an annular thread of fluid. *J. Fluid Mech.* **27**, *309-319.*

[10] Hickox, C.E. 1971 Instability due to viscosity and density stratification in axisymmetric pipe flow. it Phys. Fluids **14**, 251-262

[11] Hooper, A. P. 1985 Long-wave instability at the interface between two viscous fluids: Thin layer effects. *Phys. Fluids* **28***(6), 1613-1618.*

[12] Hooper, A. P. and Boyd, W. G. C. 1983 Shear-flow instability at the interface between two viscous fluids. *J. Fluid Mech.* **128**, *507-528.*

[13] Hu, H.H. & Joseph, D.D. 1989 Lubricated pipelines: stability of core-annular flow. Part 2. *J. Fluid Mech.* **205**, *359-396*

[14] Hu, H.H., Lundgren, T. & Joseph, D.D. 1990 Stability of core-annular flow with a small viscosity ratio. it Phys. Fluids A**2**, 1945-1954.

[15] Hyman, J.M., Nicolaenko, B. 1986 The Kuramoto-Sivashinsky equations, a bridge between PDEs and dynamical systems, *Physica D***18**, *113-126.*

[16] Hyman, J.M., Nicolaenko, B., Zaleski, S. 1986 Order and complexity in the Kuramoto-Sivashinsky model of turbulent interfaces, *Physica D***23**, *265-292.*

[17] Jolly, M.S., Kevrekides, I.G. and Titi, E.S. 1990 Approximate inertial manifolds for the Kuramoto-Sivashinsky equation: analysis and computations, *Physica D***44**, *38-60.*

[18] Joseph, D.D., Renardy, Y. & Renardy, M. 1984 Instability of the flow of immiscible liquids with different viscosities in a pipe. *J. Fluid Mech.* **141**, *309-317*

[19] Kevrekidis, I.G., Nicolaenko, B., Scovel, C. 1990 Back in the saddle again : A computer assisted study of Kuramoto-Sivashinsky equation, *SIAM J. Appl. Math.* **50**, *No. 3, 760-790.*

[20] Nicolaenko, B., Scheurer, B., Temam, R. 1985 Some Global Dynamical Properties of the Kuramoto-Sivashinsky Equation: Nonlinear Stability ans Attractors, *Physica D***16** *155-183.*

[21] Papageorgiou D.T., Maldarelli C. & Rumschitzki D.S. 1990 Nonlinear interfacial stability of core-annular flows. *Phys. Fluids* **A** *Vol. 2 Part 3, 340-352.*

[22] Papageorgiou D.T. & Smyrlis, Y.S. 1991 The route to chaos for the Kuramoto-Sivashinsky equation. *Theoret. Comput. Fluid Dynamics* **3**, *15-42.*

[23] Preziosi,L., Chen, K. & Joseph, D.D. 1989 Lubricated pipelines: Stability of core-annular flow. *J. Fluid Mech.* **201**, *323-356.*

[24] Renardy, Y. 1985 Instability at the interface between two shearing fluids in a channel. *Phys. Fluids* **28***(12), 3441-3443.*

[25] Renardy, Y. 1987 The thin-layer effect and interfacial stability in a two-layer Couette flow with similar liquids. *Phys. Fluids* **30***(6), 1627-1637.*

[26] Sivashinsky, G.I., Michelson, D.M. 1980 On irregular wavy flow of a liquid down a vertical plane, *Prog. Theor. Phys.* **63**, *2112-2114.*

[27] Smyrlis, Y.S. & Papageorgiou, D.T. 1991 Predicting chaos for infinite-dimensional dynamical systems: the Kuramoto-Sivashinsky equation, a case study. *Proc. Nat. Acad. Sciences, USA* **88** *No. 24, 11129-11132.*

[28] Tomotika, S. 1935 On the stability of a cylindrical thread of a viscous liquid surrounded by another viscous fluid. *Proc. Roy. Soc. Lond. A***150**, *322-337.*

[29] von Kerczek, C. H. 1987 Stability characteristics of some oscillatory flows - Poiseuille, Ekman and films. In Stability of Time Dependent and Spatially Varying Flows, D.L. Dwoyer and M.Y. Hussaini, eds, Springer-Verlag.

[30] Yih, C.-S. 1967 Instability due to viscosity stratification. *J. Fluid Mech.* **27**, *337-352.*

[31] Yih, C.-S. 1968 Instability of unsteady flows or configurations Part 1. Instability of a horizontal liquid layer on an oscillating plate. *J. Fluid Mech.* **31**, *737-751.*

A Analysis of the numerical data

The diagnostics we use are aimed at the determination of the type of attractors present. To do this we first begin with the L^2-norm (or energy) of the solution define d by

$$E(t) = \frac{1}{2\pi}\int_0^{2\pi} u^2(t,x)dx,$$

and which can be computed along with the solution. For example, in the odd-parit y case we have

$$E(t) = \frac{1}{2}\sum_1^N a_k^2(t),$$

with analogous expressions in the general case. Of concern is the behavior of $E(t)$ for large t. If $E(t)$ tends to a non-zer o constant as $t \to \infty$, for example, then $u(t,x)$ tends to a non-uniform stationary or travell ing steady state. Time periodicity in the fourier coefficients (and consequently in $u(t,x)$) show s up as a time periodicity in $E(t)$. A useful way to confirm such periodic flows is to constru ct numerically the phase-plane of $(E, \dot{E})$; the index of the closed curve determines the numbe r of maxima and minima of $E(t)$ over one period and can be used with good accuracy to follow pe riod-doubling bifurcations, for instance, as in (SP) where as many as thirteen bifurcations we re analyzed this way.

When the dynamics gets more complicated and chaotic, the phase plane may gain mo re and more turns as the dynamics enter a strange attractor, fill out whole regions of the (E, tE) plane as t increases as for quasi-periodic oscillations for instance, or produce dynami cs which are both random and unrecognizable. In all these cases it is difficult to infer with much certainty what is happening and a more accurate test is needed. One diagnostic we found to be very useful is the return map described below.

A return map can be constructed as follows. Given the time history of $E(t)$ (th e non-constant state is the interesting one), and the phase plane described above, Poincaré secti ons can be constructed in the usual way. In particular the minima and maxima of $E(t)$ are Poincaré sections having $\dot{E} = 0$ and $\frac{d^2E}{dt^2}$ negative and positive respectively. For def initeness consider the minima of $E(t)$ from a given point in time (large enough for transients to be unimportant) onwards and define them by the infinite sequence $\{E_n\}_1^\infty$. The return map of these values, which gives a picture of the attractor in that i t is a construction of the map (it may not necessarily be a function) necessary to reproduce the flo w, is obtained by collectively plotting the pairs points $\{(E_k, E_{k+1})\}_{k=1}^{\in} fty$ in the plane. In practice we do not compute an infinite number of minima but must nonetheless compute enough to provide a picture of the dynamics. In addition is is essential that the values o f the minima be found with enough accuracy from the computation - see accuracy requirements belo w.

The simple example of the logistic map serves as a useful illustration of the ab ove construction. The logistic map produces a sequence of iterates $\{x_n\}_1^\infty$ from the quadratic formula $x_{n+1} = 4\mu x_n(1 - x_n) \equiv f(x_n)$ with $0 < \mu < 1$ a parameter. A gr aphical iteration starting from some initial value produces the desired sequence (see Devaney for instance) . This iteration and proceeds as follows: Start from a given point x_k say; the iterate of x_k is $x_{k+1} = f(x_k)$ whose value is the length of the vertical line joining x_k to the curve; the iterate of x_{k+1} is found by moving horizontally from the point (x_k, x_{k+1}) to the line of unit slope through the origin, and then vertically up to the curve and the process can be repeated *ad infinitum*. Collectively, then, the points $\{(x_k, x_{k+1})\}_{k=1}^\infty$ are drawn in the plane and all lie on the parabola of the logistic map. The construction of the return map from a sequence such as $\{E_n\}_1^\infty$ duplicates exactly this graphical iteration and constructs the unknown curve $f(x)$, if it exists, or a more complicated object such as a strange attractor for

instance. Such return map diagnostics have been used extensively by experimentalists - see Bergé et al. for numerous examples.

The interpretation of the return map is usually quite clear provided the minima have been determined accurately. There are five distinct pictures which we have encountered in our numerical work on the KS and the OSCKS based on the r eturn map of the minima of $E(t)$ and which are interpreted as follows as far as the dynamics of $E(t)$ are concerned:

1. One or more fixed points in the plane - time periodic flow with a number o f minima equal to the number of fixed points.
2. An open curve in the plane which may or may not be a single valued functio n - chaotic flow as would be obtained from the logistic map for instance (the former case), or ju st after the Feigenbaum cascade to chaos for the KS equation (see PS, SP).
3. An open curve which is highly folded and which exhibits self-similar behav ior at smaller scales - chaotic flow with a strange attractor of dimension between 1 and 2 reme niscent of the Hénon map - such behavior has been found by Papageorgiou & Smyrlis (1994) f or the KS equation far from the Feigenbaum cascade.
4. One or more closed curves with no folding - quasi-periodic flow as reporte d in several examples in the present article.
5. Unrecognizable pattern which fills out regions of the plane - we term this type of flow as unrecognizable chaos and several examples are given here and in Papageorgiou & Smyrlis (1994) for the KS equation.

Finally we make a comment about the need of high accuracy requirements. As an il lustration of such needs, consider a case which produces quasi-periodic oscillations in $E(t)$. $E(t)$ is numerically computed at intervals separated by the time-step Δt. In many problems a large Δt can be used to compute the flow accurately. The simplest approach of finding the energy minima is to dynamically track the minimum value and store it when found; the error associ ated with this is of the order of magnitude of the local value of $\dot{E} \times \Delta t$; instea d of a closed curve of zero thickness such errors can indicate spurious behavior which can be of the same size as real phenomena (this is especially true as δ_1 becomes increasingly small er and the amplitude of quasi-periodic modulations decreses). To overcome this difficulty the minima are computed dynamically in the code by a high order interpolation involving as many as 15 points, depending on the time-step, on either side of a local maximum or minimum. All results reported here have been produced by an accurate evaluation of the minima and maxima of $E(t)$ in order to produce highly accurat e and convincing return maps.

Tables

ν	N	δ_1	ω_1	Description	Figure
0.9	10	0.0	0.0	Uni-modal steady attractor	
0.9	10	0.5	1.0	Uni-modal periodic attractor, $T = 2\pi$	2
0.1	16	0.1	1.0	Bi-modal periodic attractor, $T = 2\pi$	3
0.1	16	0.1	2.0	Bi-modal periodic attractor, $T = \pi$	3
0.1	16	0.1	0.1	Bi-modal periodic attractor, $T = \pi/5$	
0.0303	20	0.0	0.0	Periodic attractor	
0.0303	20	0.01	1.0	Quasi-periodic oscillations	4(a)
0.0303	20	0.1	1.0	Quasi-periodic oscillations	4(b)
0.0303	20	0.5	1.0	Periodic attractor, $T = 2\pi$	4(c)
0.0215	24	0.0	0.0	Chaotic oscillations	
0.0215	24	0.1	1.0	Chaotic oscillations	
0.0215	24	0.5	1.0	Chaotic oscillations	

Table 1 : Overview of solutions of the OSCKS with sinusoidal profile.

ν	N	δ_1	ω_1	Description	Figure
0.3	12	0.0	0.0	Traveling wave	5(a)
0.3	12	0.01	1.0	Quasi-periodic traveling wave	5(b)
0.3	12	0.1	1.0	Quasi-periodic traveling wave	5(c)
0.3	12	0.5	1.0	Quasi-periodic traveling wave	
0.22	16	0.0	0.0	Periodic homoclinic bursting	6(a)
0.22	16	0.1	1.0	Chaotic oscillations	6(b)
0.136	16	0.0	0.0	Bi-modal steady attractor	
0.136	16	0.0	1.0	Modulated bi-modal attractor	
0.1212	20	0.0	0.0	Chaotic oscillations/Strange attractor	7(a) & 7(aa)
0.1212	16	0.1	1.0	Chaotic oscillations	7(b)
0.1212	16	0.5	1.0	Chaotic oscillations	
0.085	16	0.0	0.0	Chaotic oscillations	
0.085	16	0.1	1.0	Chaotic oscillations	

Table 2 : Overview of solutions of the OSCKS with mixed profile.

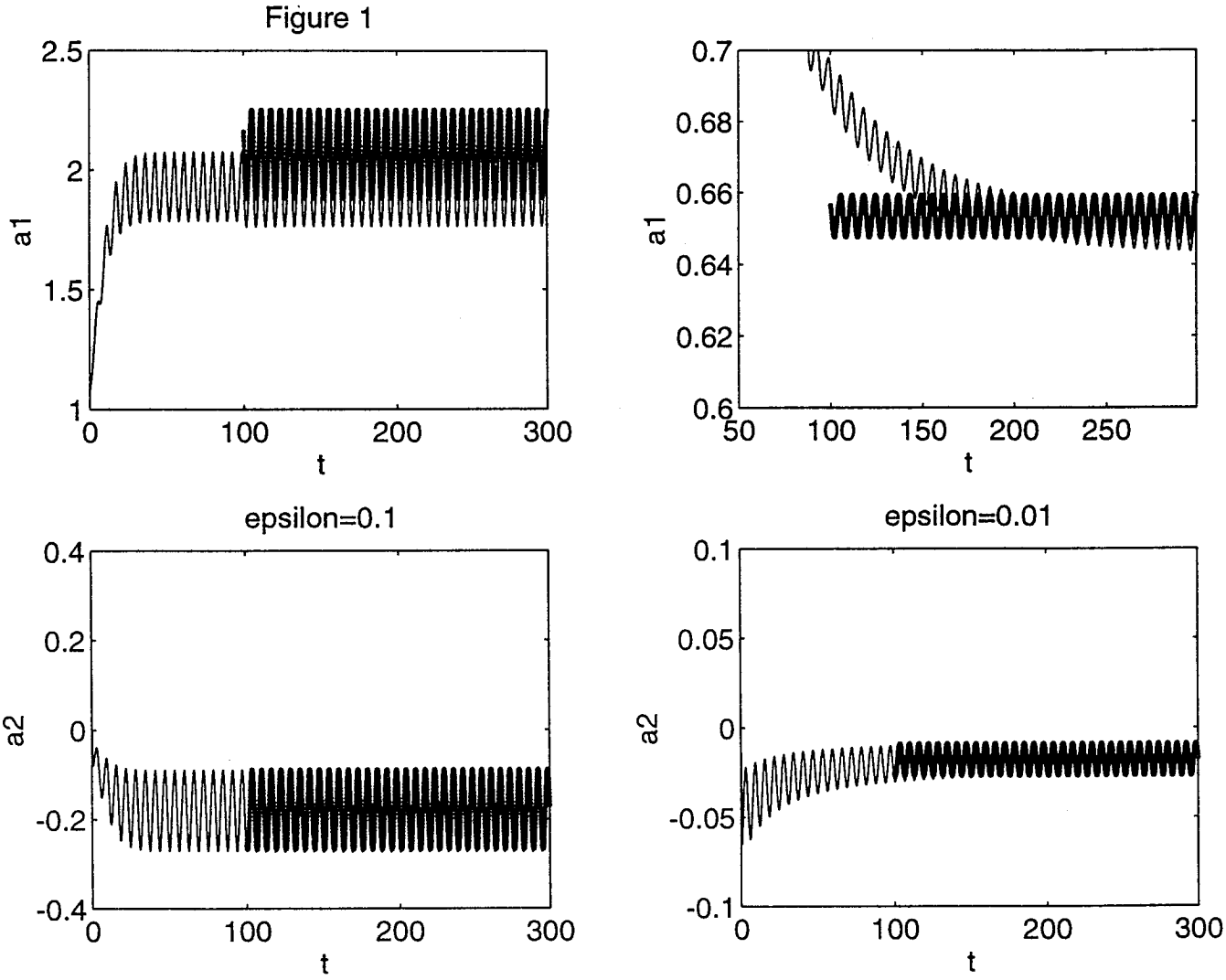

1 Comparison of asymptotic and numerical solutions of the OSCKS equation with ν near 1, $\delta_1 = 0.5$, $\omega_1 = 1.0$. The fourier coefficients $a_1(t)$ and $a_2(t)$ for $\epsilon = 1 - \nu = 0.1, 0.01$; dark line - asymptotic result (48a-c).

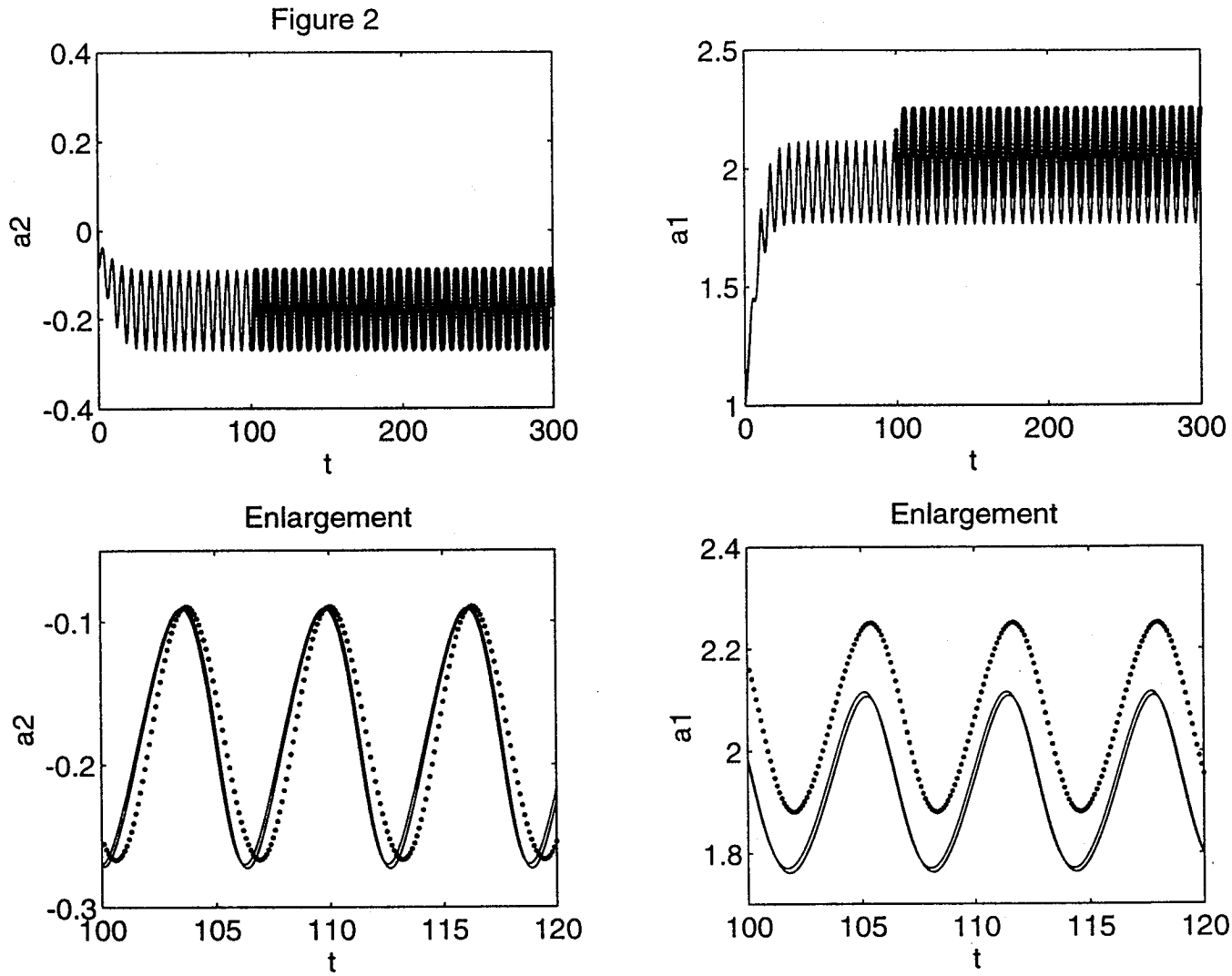

2 As in Figure 1 but computation with 2 modes and 20 modes as well as asymptotic result (dark (dotted) line).

Figure 3

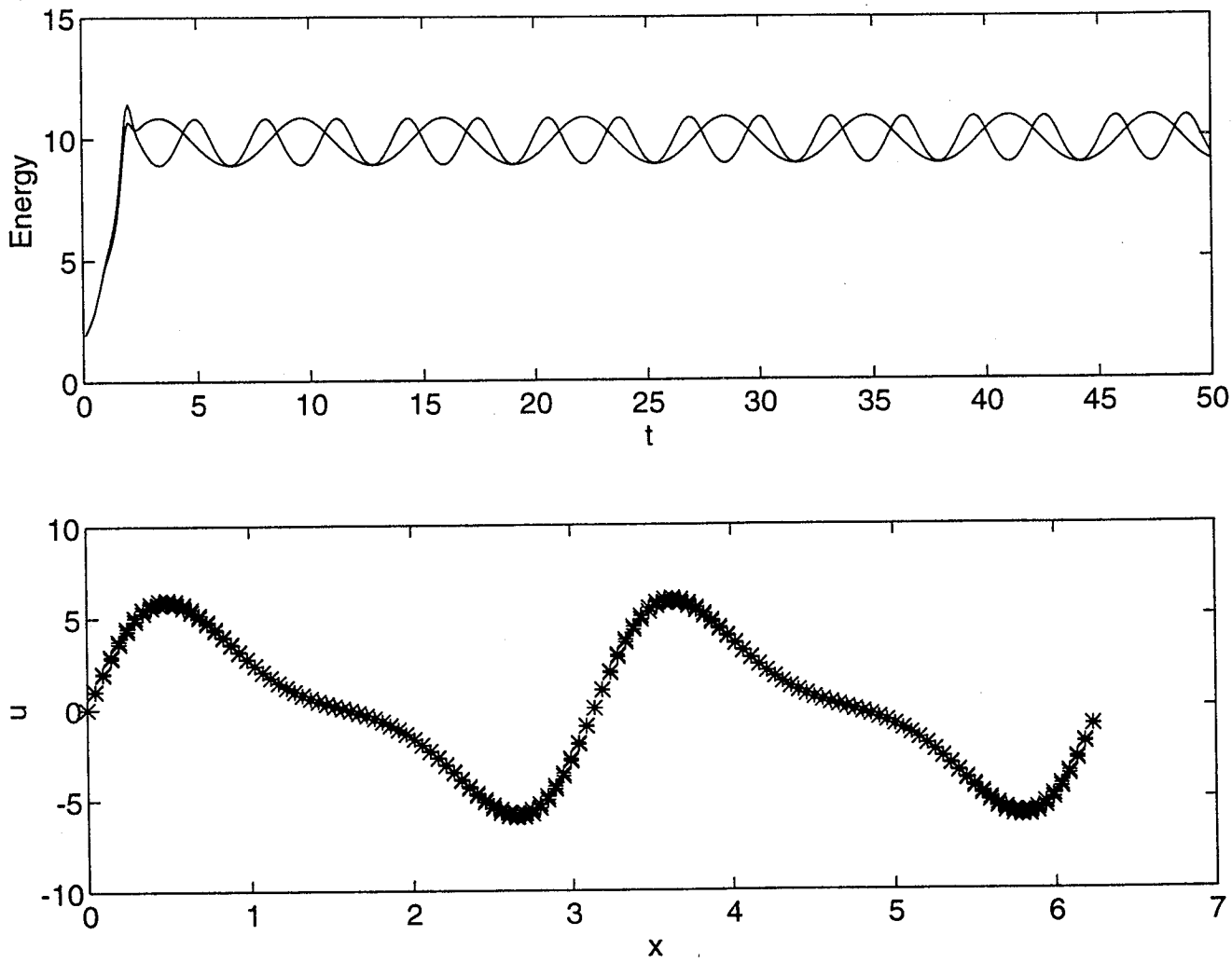

3 OSCKS equation: Bi-modal periodic attractor, with $\nu = 0.1$, $\delta_1 = 0.1$, $\omega_1 = 1, 2$. Energy against time, and the spatial structure of the profile.

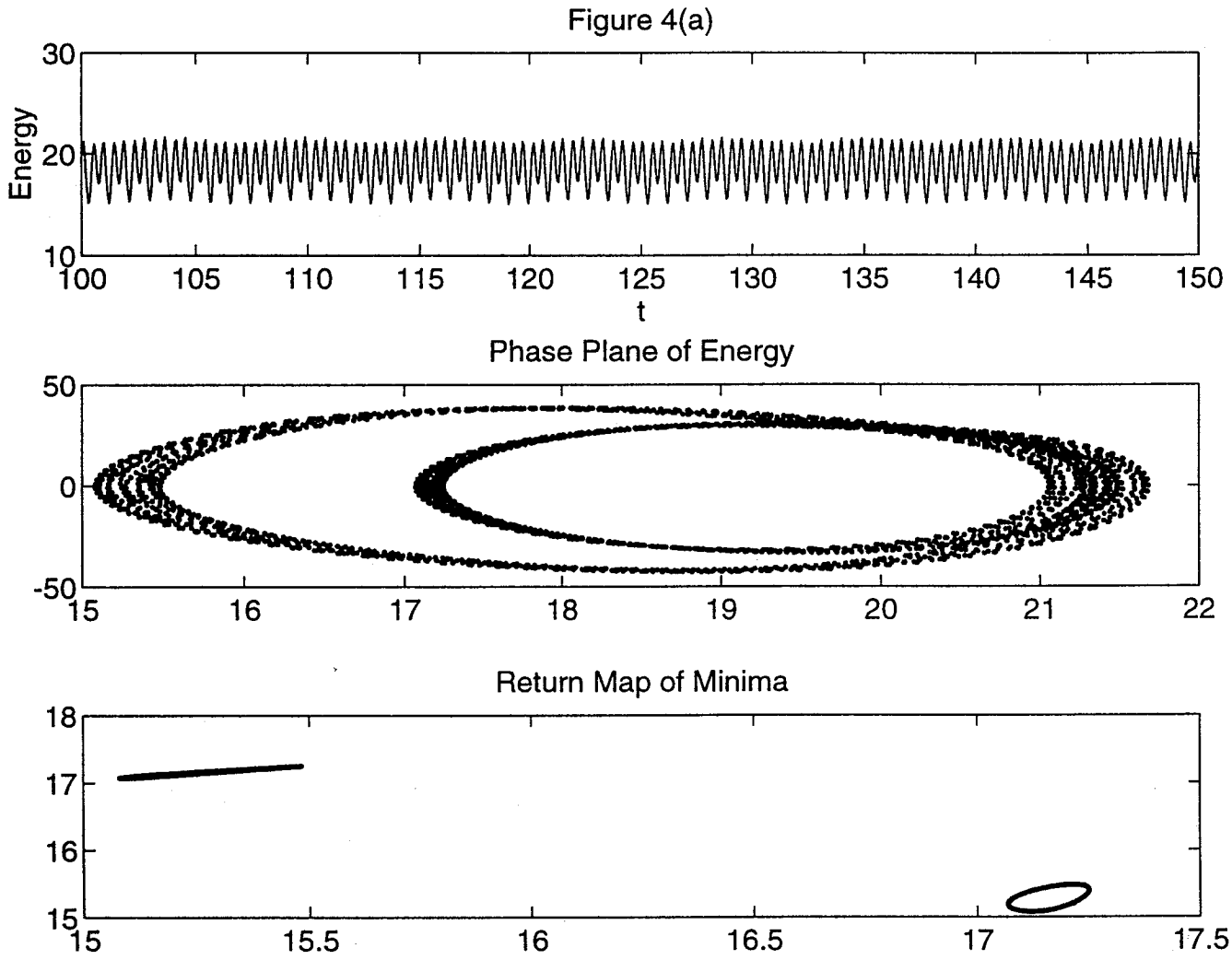

4(a) OSCKS equation: quasi-periodic oscillations, with $\nu = 0.0303$, $\delta_1 = 0.01$, $\omega_1 = 1.0$.

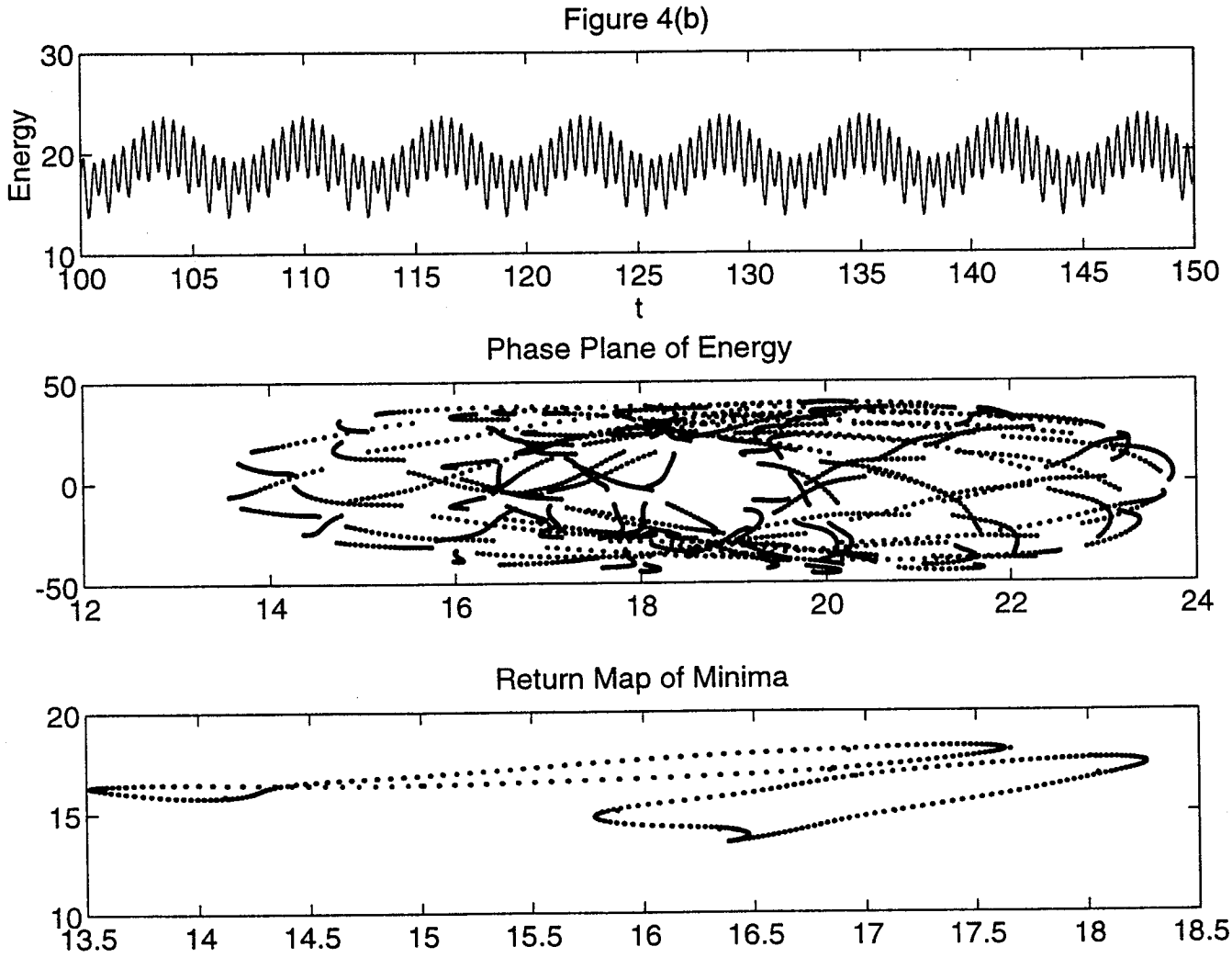

4(b) OSCKS equation: quasi-periodic oscillations, with $\nu = 0.0303$, $\delta_1 = 0.1$, $\omega_1 = 1.0$.

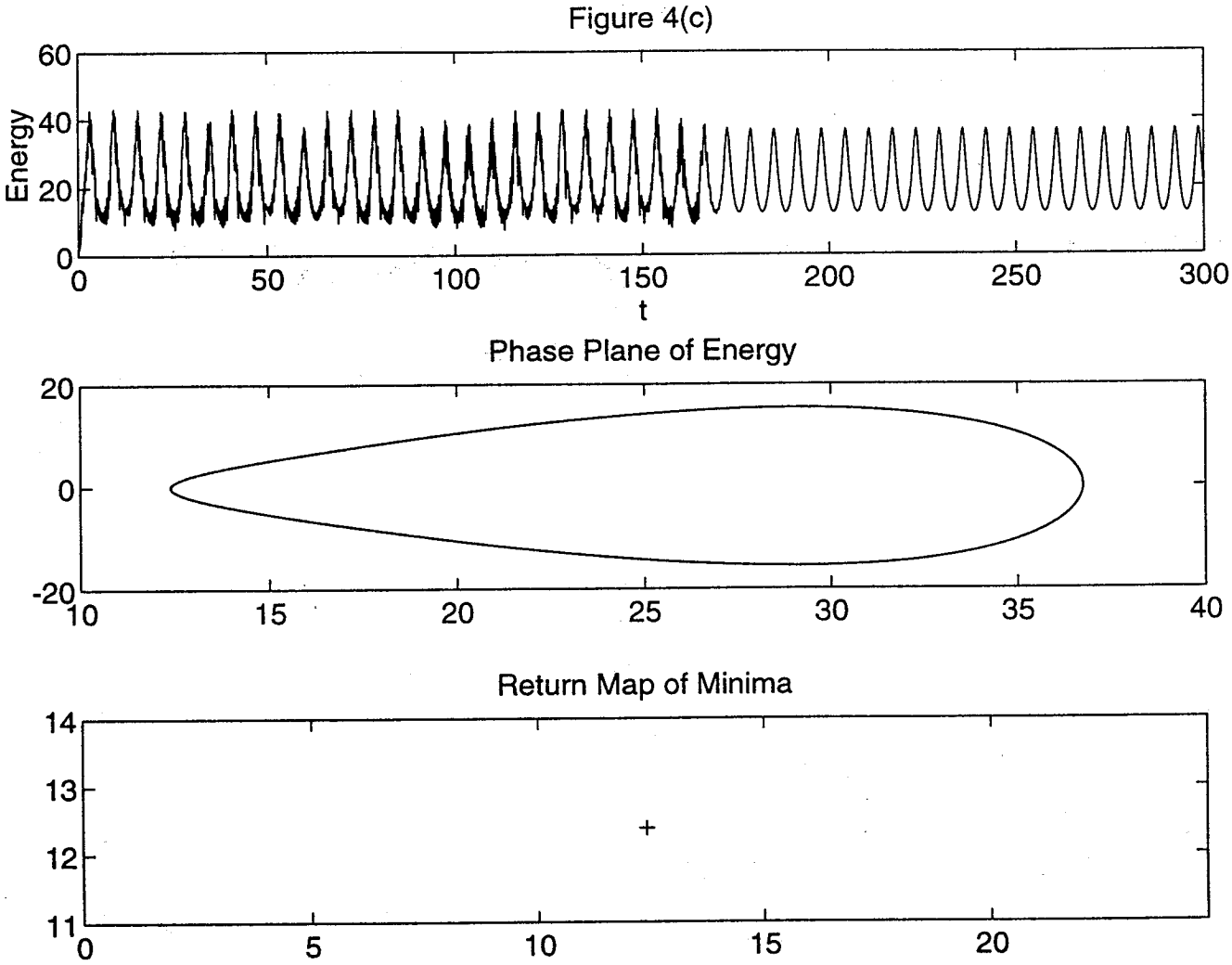

4(c) OSCKS equation: quasi-periodic oscillations initially and later frequency locking to time-periodic state, with $\nu = 0.0303$, $\delta_1 = 0.5$, $\omega_1 = 1.0$. The KS in 4(a)-(c) has a time-periodic attractor of period ~ 0.89.

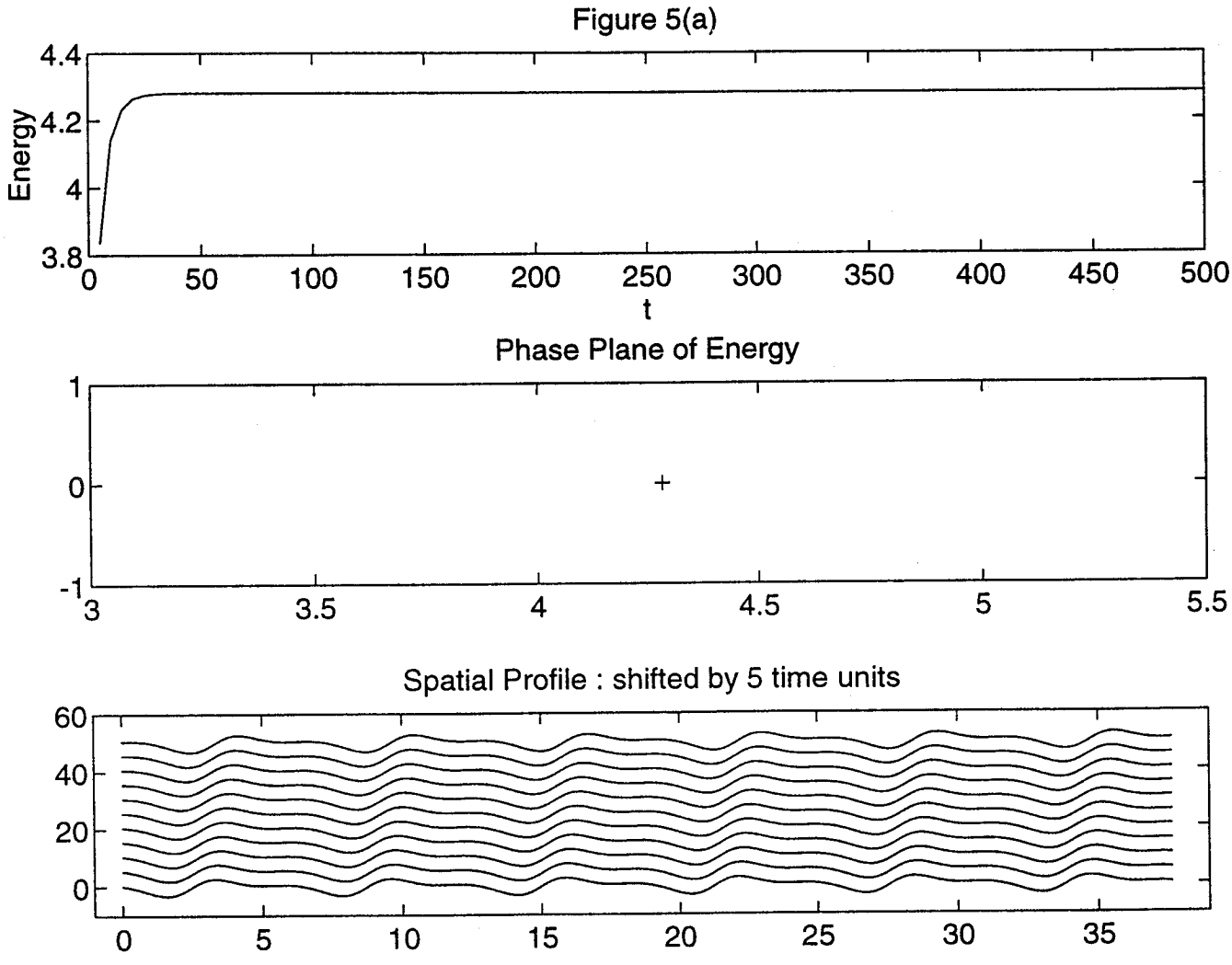

5(a) KS equation with general initial data: travelling wave with $\nu = 0.3$; unimodal attractor.

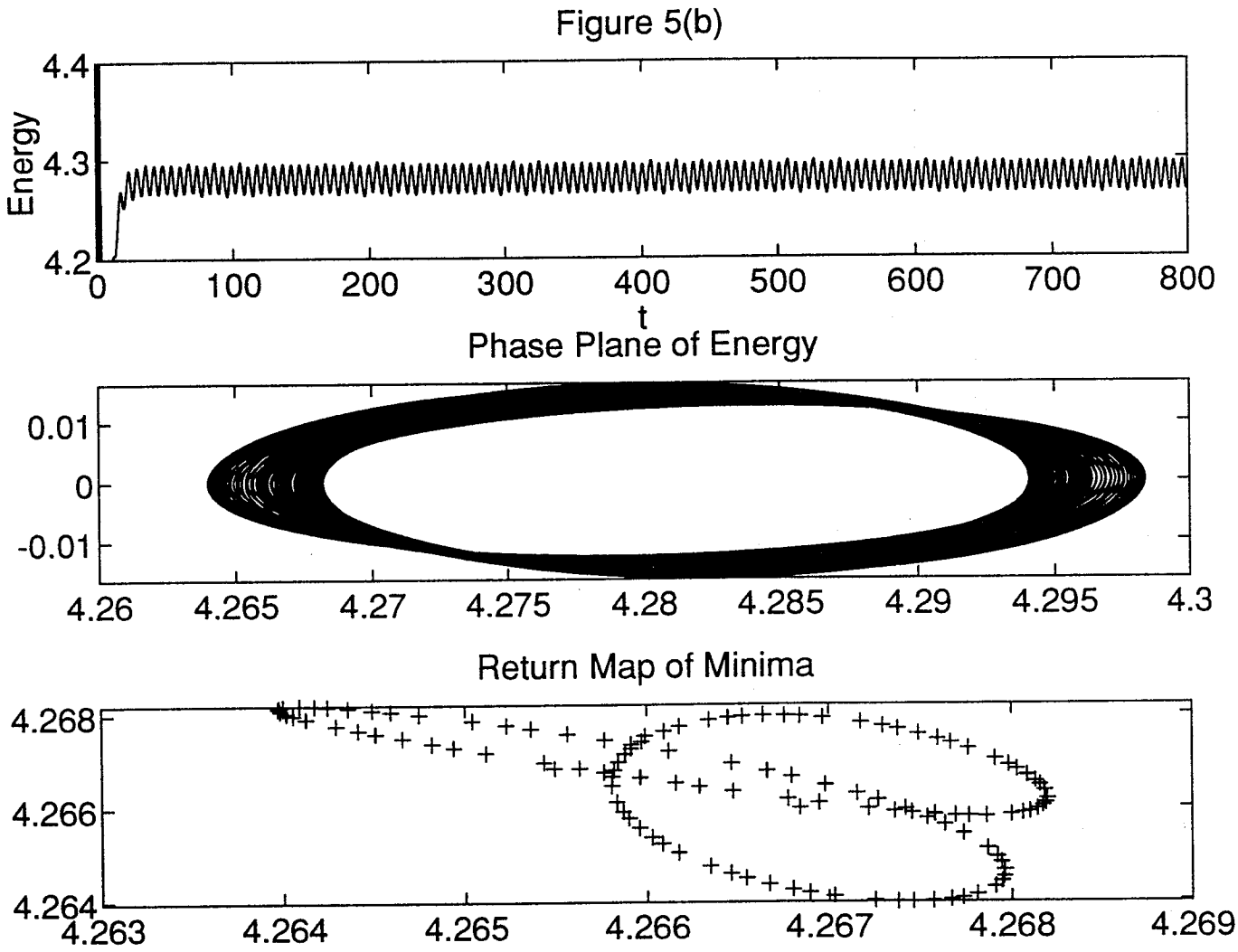

5(b) OSCKS equation: quasi-periodic travelling wave, $\nu = 0.3$, $\delta_1 = 0.01$, $\omega_1 = 1.0$.

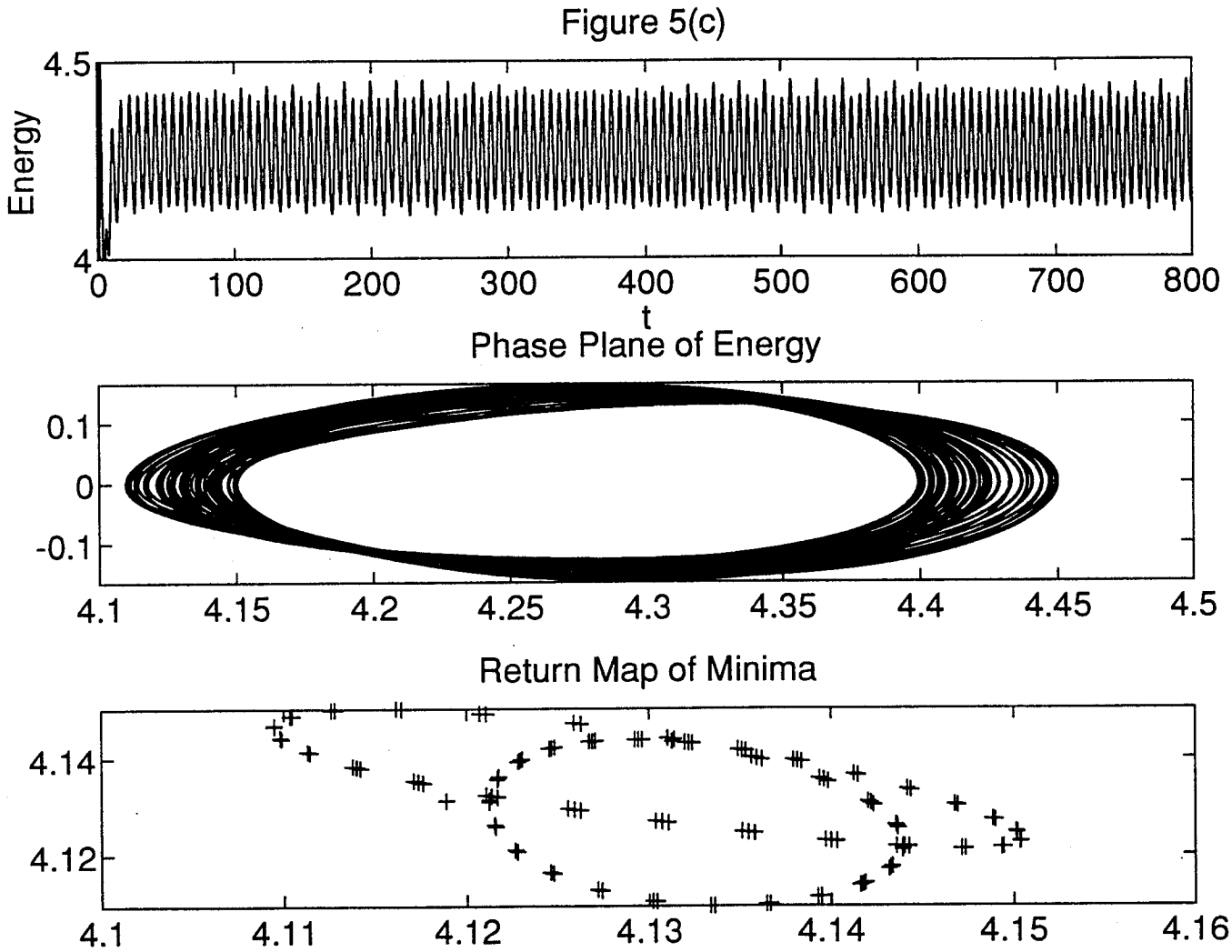

5(c) OSCKS equation: quasi-periodic travelling wave, $\nu = 0.3$, $\delta_1 = 0.1$, $\omega_1 = 1.0$.

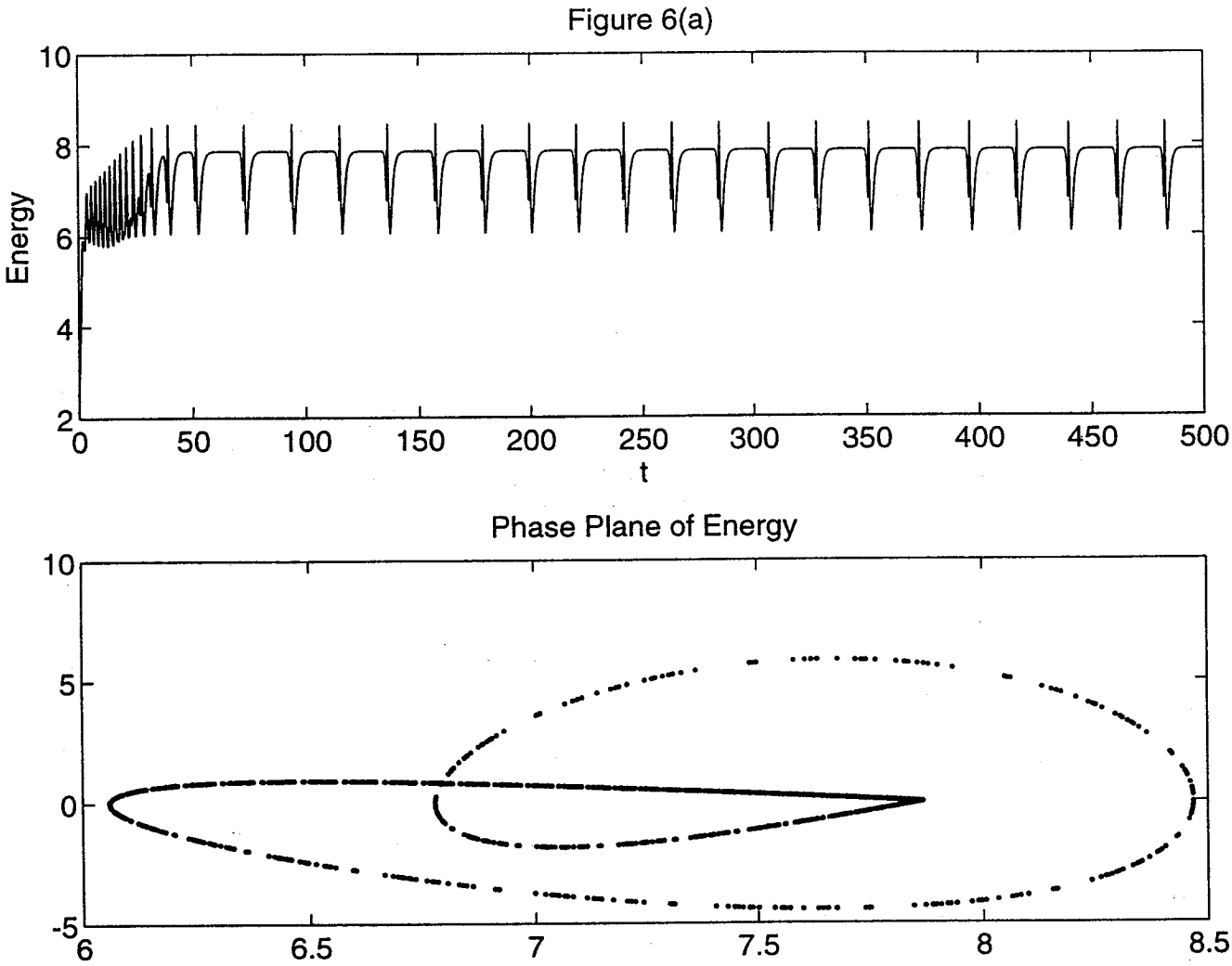

6(a) KS equation: periodic homoclinic bursts, $\nu = 0.22$.

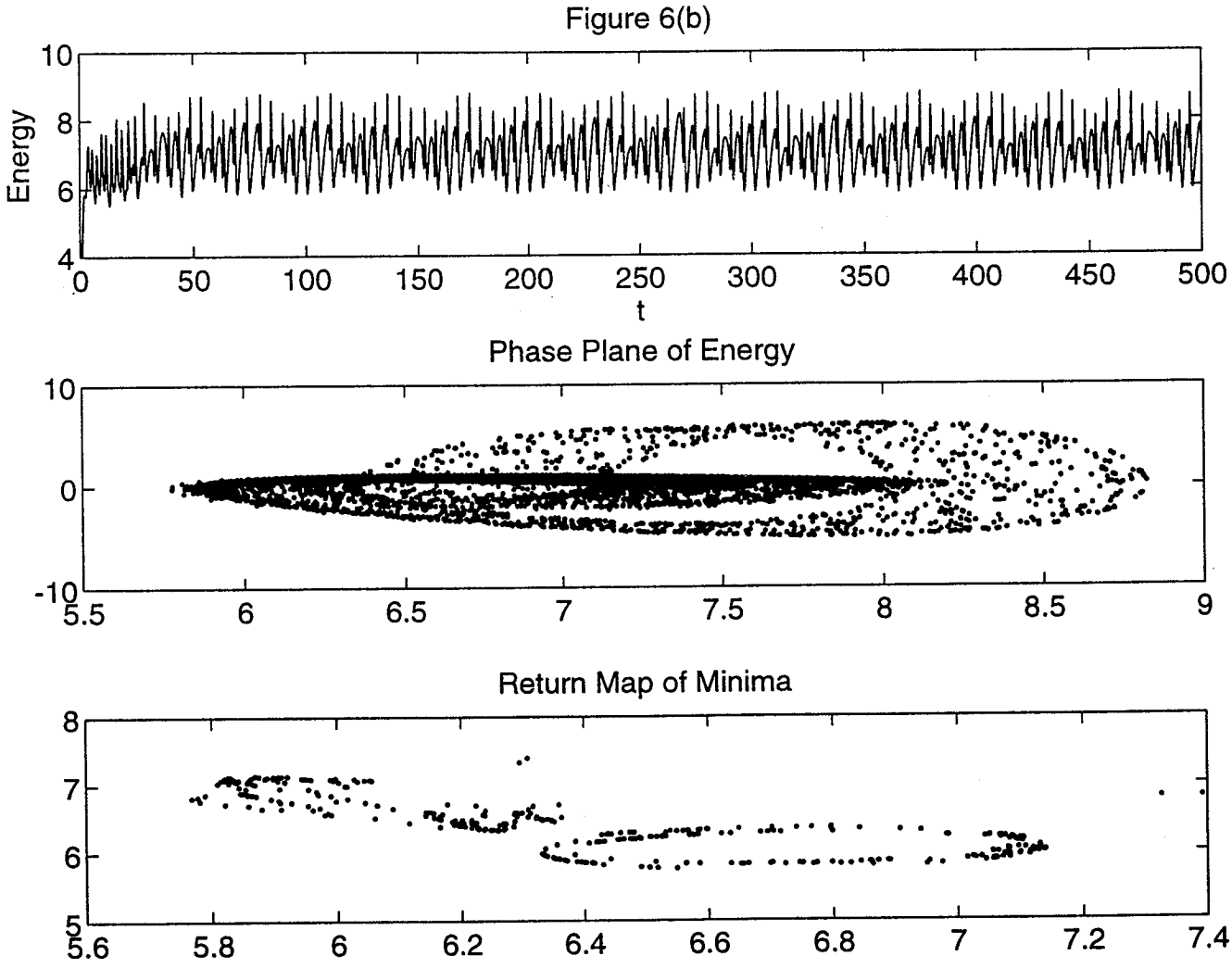

6(b) OSCKS equation: chaotic oscillations (almost quasi-periodic attractor), $\nu = 0.22$, $\delta_1 = 0.05$, $\omega_1 = 1.0$.

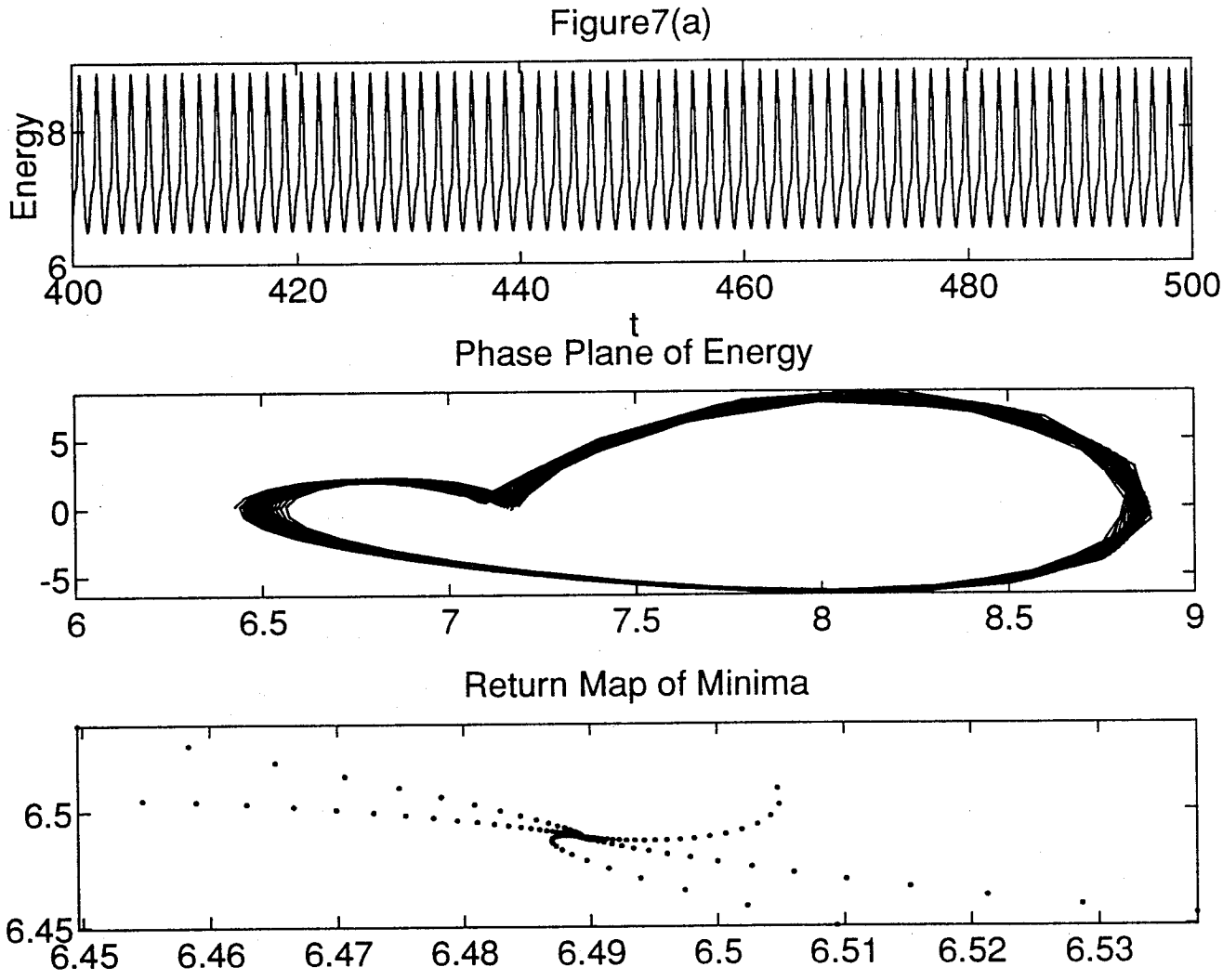

7(a) KS equation: Chaos just beyond a period-doubling cascade; strange attractor, $\nu = 0.1212$.

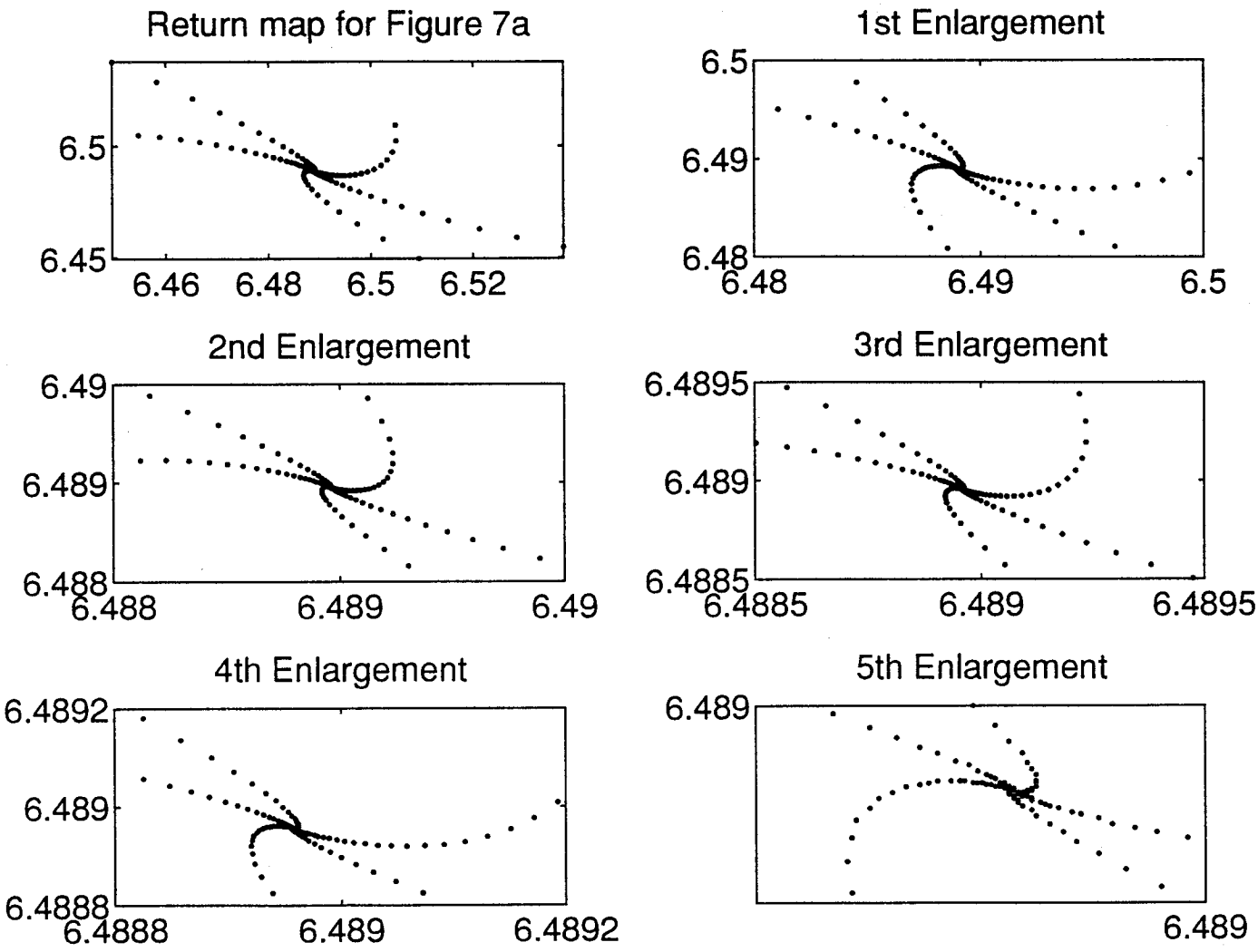

7(aa) Enlargement of returm map showng the self-similar nature of the strange attractor; $\nu = 0.1212$. Overall enlargement factor is 1.2×10^3.

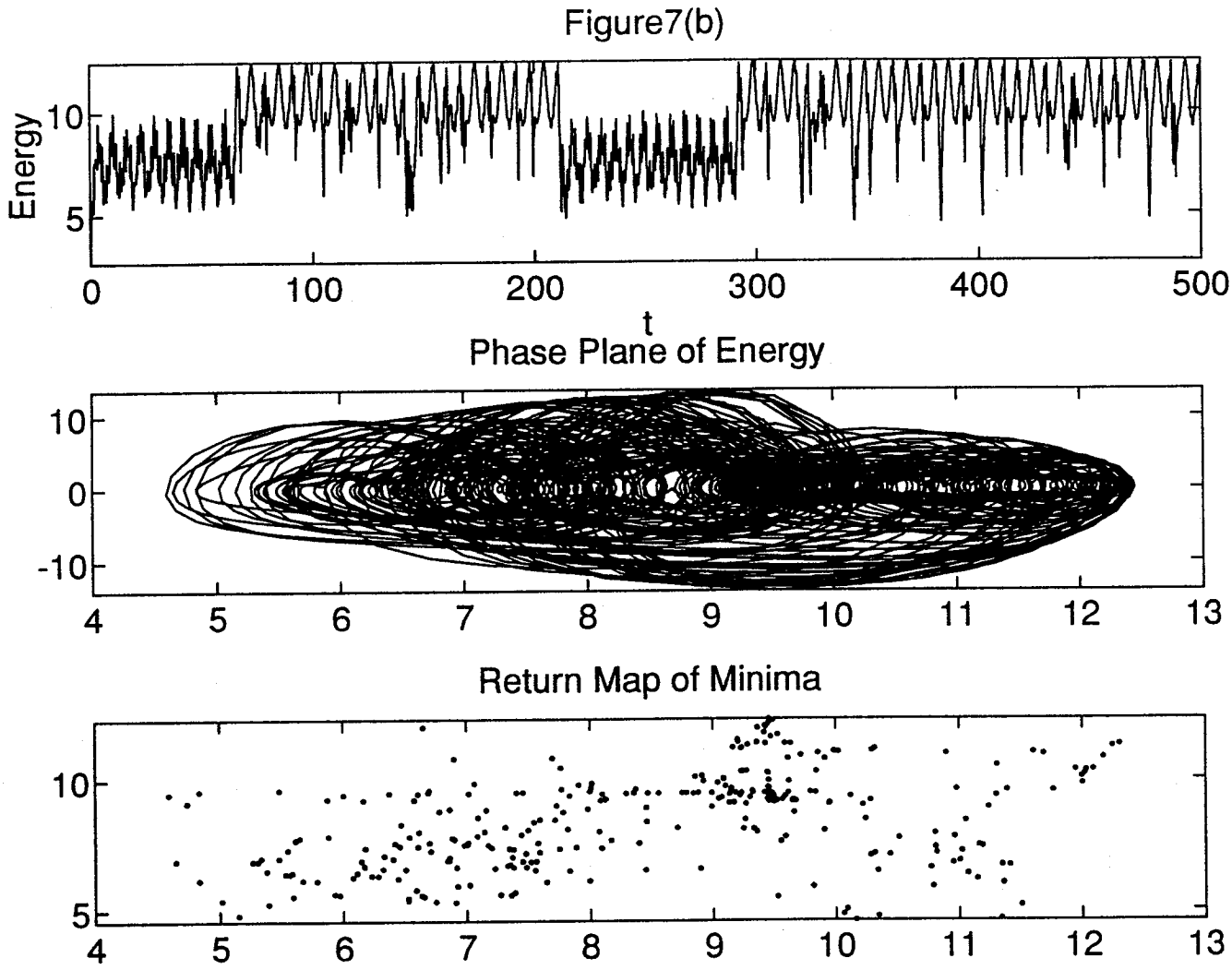

7(b) OSCKS equation: chaotic oscillations, with $\nu = 0.1212$, $\delta_1 = 0.1$, $\omega_1 = 1.0$.

Figure 8

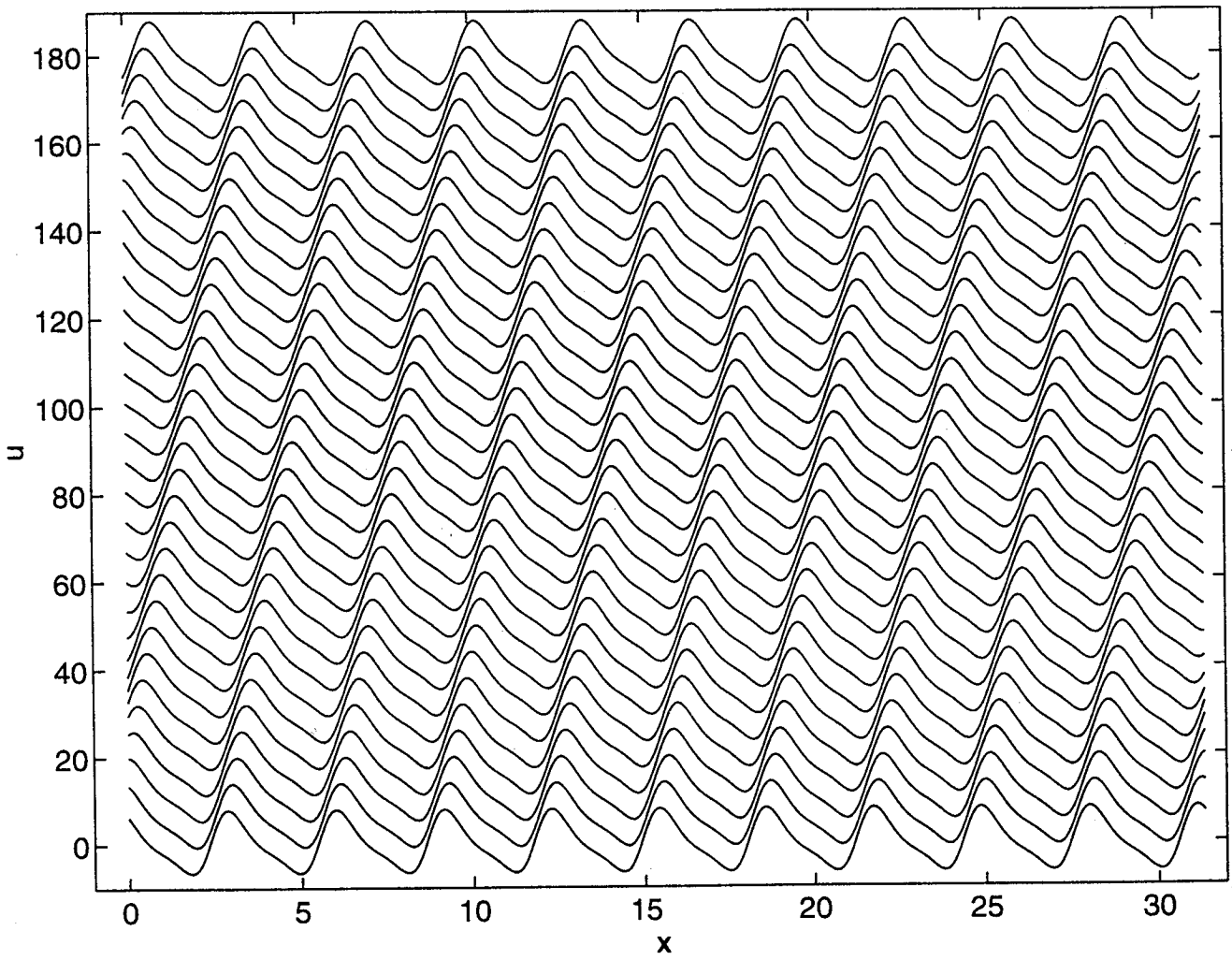

8 Modified KS equation with viscosity stratification, $m = 3.0$, $\nu = 0.1212$ ($\delta_1 = 0$). Steady-state travelling wave.

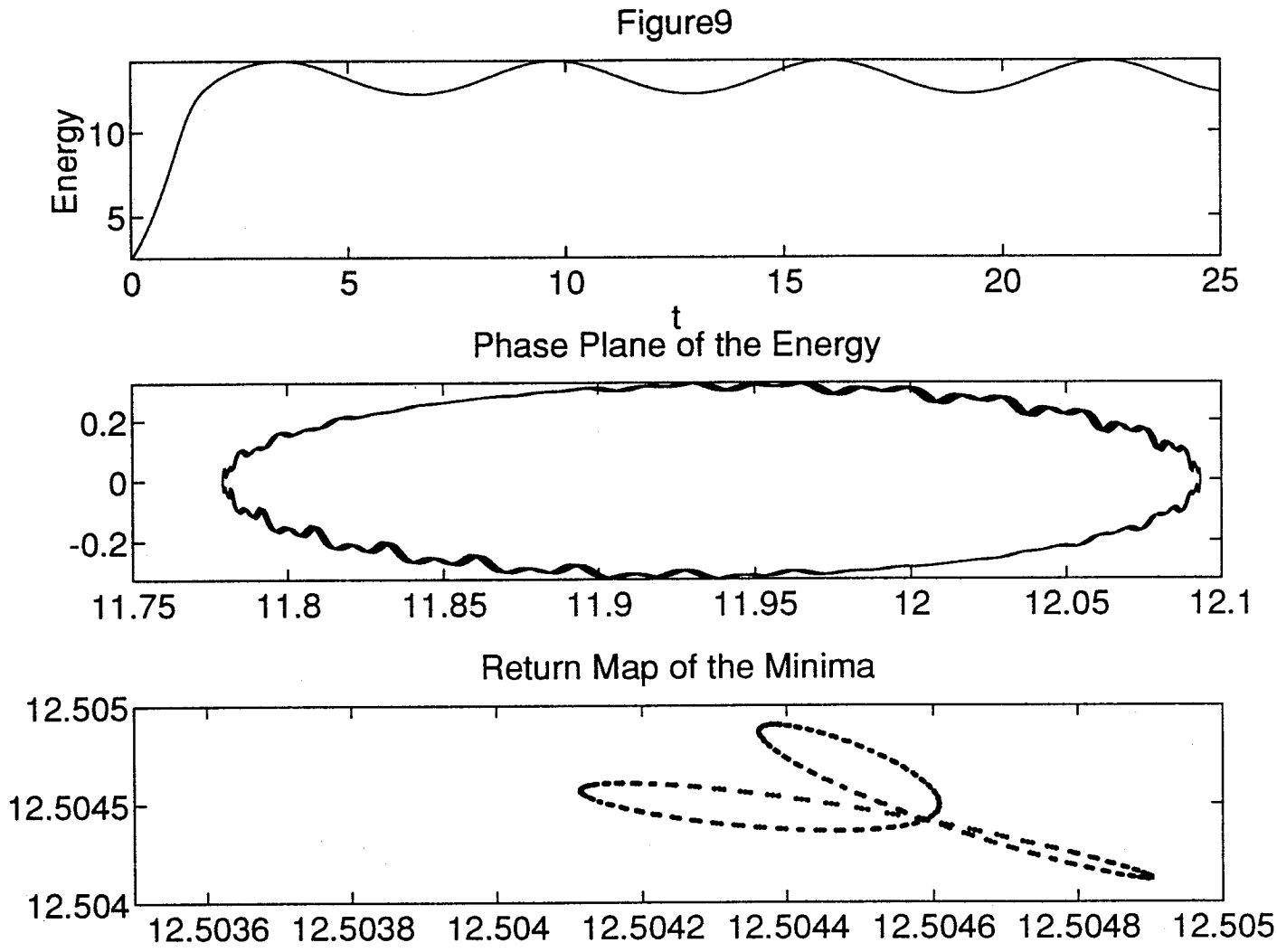

9 Modified OSCKS equation with viscosity stratification, $m = 3.0$, $\nu = 0.1212$, $\delta_1 = 0.1$, $\omega_1 = 1.0$. Quasi-periodic attra ctor.

Figure 10

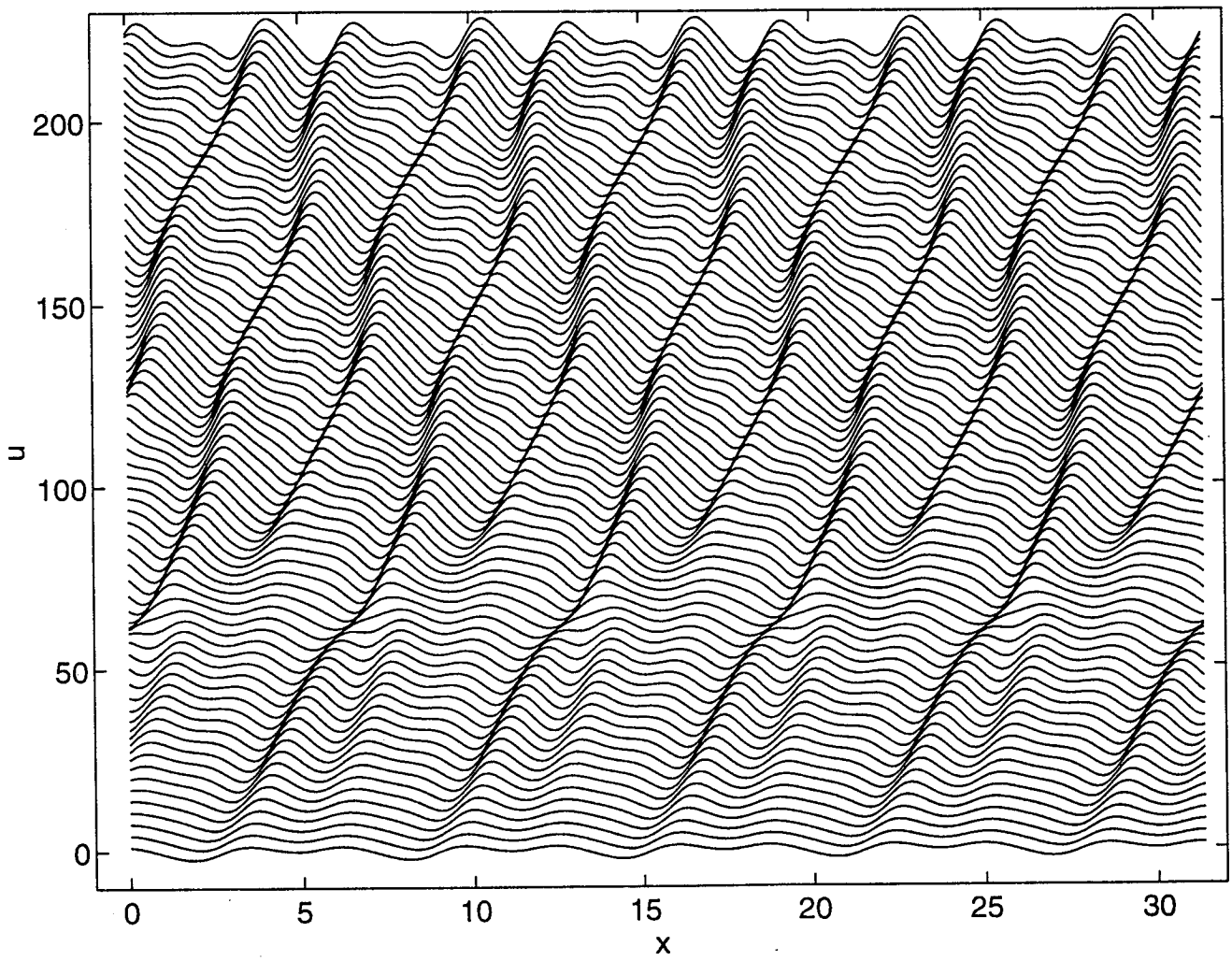

10 Modified OSCKS equation with viscosity stratification: spatial evolution of quasi-periodic travelling wave, $m = 3.0$, $\nu = 0.1212$, $\delta_1 = 0.1$, $\omega_1 = 1.0$.

REPORT DOCUMENTATION PAGE

Form Approved
OMB No. 0704-0188

1. AGENCY USE ONLY *(Leave blank)*	2. REPORT DATE	3. REPORT TYPE AND DATES COVERED
	July 1994	Contractor Report

4. TITLE AND SUBTITLE
NONLINEAR STABILITY OF OSCILLATORY CORE-ANNULAR FLOW: A GENERALIZED KURAMOTO-SIVASHINSKY EQUATION WITH TIME PERIODIC COEFFICIENTS

5. FUNDING NUMBERS
C NAS1-19480
WU 505-90-52-01

6. AUTHOR(S)
Adrian V. Coward
Demetrios T. Papageorgiou
Yiorgos S. Smyrlis

7. PERFORMING ORGANIZATION NAME(S) AND ADDRESS(ES)
Institute for Computer Applications in Science
and Engineering
Mail Stop 132C, NASA Langley Research Center
Hampton, VA 23681-0001

8. PERFORMING ORGANIZATION REPORT NUMBER
ICASE Report No. 94-47

9. SPONSORING/MONITORING AGENCY NAME(S) AND ADDRESS(ES)
National Aeronautics and Space Administration
Langley Research Center
Hampton, VA 23681-0001

10. SPONSORING/MONITORING AGENCY REPORT NUMBER
NASA CR-194933
ICASE Report No. 94-47

11. SUPPLEMENTARY NOTES
Langley Technical Monitor: Michael F. Card
Final Report
Submitted to ZAMP

12a. DISTRIBUTION/AVAILABILITY STATEMENT
Unclassified–Unlimited
Subject Category 34

12b. DISTRIBUTION CODE

13. ABSTRACT *(Maximum 200 words)*

In this paper the nonlinear stability of two-phase core-annular flow in a pipe is examined when the acting pressure gradient is modulated by time harmonic oscillations and viscosity stratification and interfacial tension is present. An exact solution of the Navier-Stokes equations is used as the background state to develop an asymptotic theory valid for thin annular layers, which leads to a novel nonlinear evolution describing the spatio-temporal evolution of the interface. The evolution equation is an extension of the equation found for constant pressure gradients and generalizes the Kuramoto-Sivashinsky equation with dispersive effects found by Papageorgiou, Maldarelli & Rumschitzki, Phys. Fluids A 2(3), 1990, pp.340-352, to a similar system with time periodic coefficients. The distinct regimes of slow and moderate flow are considered and the corresponding evolution is derived. Certain solutions are described analytically in the neighborhood of the first bi furcation point by use of multiple scales asymptotics. Extensive numerical experiments, using dynamical systems ideas, are carried out in order to evaluate the effect of the oscillatory pressure gradient on the solutions in the presence of a constant pressure gradient.

14. SUBJECT TERMS	15. NUMBER OF PAGES
trailing-line vortex, viscous compressible stability	44
	16. PRICE CODE: A03

17. SECURITY CLASSIFICATION OF REPORT	18. SECURITY CLASSIFICATION OF THIS PAGE	19. SECURITY CLASSIFICATION OF ABSTRACT	20. LIMITATION OF ABSTRACT
Unclassified	Unclassified		

NSN 7540-01-280-5500

Standard Form 298(Rev. 2-89)
Prescribed by ANSI Std. Z39-18
298-102

☆U.S. GOVERNMENT PRINTING OFFICE: 1994 - 528-064/23019